TOMMI REINIKKA
IMPLEMENTATION OF ONLINE IMPEDANCE MEASURE-
MENT SETUP FOR THREE-PHASE GRID-CONNECTED IN-
VERTERS

Master of Science Thesis

ABSTRACT

In the thesis a fast method for measuring the output impedance of a grid-connected inverter by broadband excitation and cross-correlation techniques is studied. The study is made for determining stability of a grid-connected power electronics system by using impedance based stability criterion. The goal of this work is to build a test bench for inverter experiments and to verify the accuracy of the used measurement technique.

Renewable power generation, such as solar and wind power, require a way to synchronize and connect to the grid. This is usually done by using grid-parallel inverters. However impedance mismatch between the grid and the interfacing inverter may cause the inverter to generate harmonic resonances. The resonance problems can be analyzed and prevented using analytical inverter models or measured frequency responses. In this thesis pseudo-random sequences and grid emulator are used to measure the inverter output impedance at a high frequency band.

The experiments were done by injecting the pseudo-random binary sequence signal into the grid voltage reference. The grid voltages and currents were measured and used to calculate the inverter's frequency response with voltage as the input and current as the output. The measurements were verified by comparing them to theoretical values.

The method used in the thesis can be applied for verifying inverter impedance models and for studying the dynamic behavior of the inverter control. The experiments show that the method is accurate over a wide frequency band, it is fast to use and easy to tune for the required measurements.

TIIVISTELMÄ

TOMMI REINIKKA: Online impedanssin mittausjärjestelmän toteuttaminen kolmivaiheiselle verkkoon kytketylle vaihtosuuntaajalle
Tampereen teknillinen yliopisto
Diplomityö, 54 sivua
maaliskuu 2017
Sähkötekniikan koulutusohjelma
Pääaine: Tehoelektroniikka
Ohjaaja: Akatemiatutkija Tomi Roinila
Tarkastajat: Assistant Prof. Tuomas Messo

Avainsanat: tehoelektroniikka, verkkostabiilius, taajuusvaste, pseudosatunnainen binäärijakso, impedanssiperusteinen stabiilius

Diplomityössä tutkitaan keinoa mitata nopeasti verkkoon kytketyn vaihtosuuntaajan ulostuloimpedanssi käyttämällä laajakaistaherätteitä ja ristikorrelaatiomenetelmiä. Työn tavoitteena on rakentaa testipenkki vaihtosuuntaajatesteille ja varmistaa mittaustavan tarkkuus.

Uusiutuvat energian tuotantomuodot, kuten aurinko- ja tuulivoima, tarvitset tavan synkronoida ja yhdistää energialähde sähköverkon kanssa. Tämä tehdään liittämällä tehontuotanto verkkoon käyttämällä verkkoon rinnankytkettyjä vaihtosuuntaajia. Vaihtosuuntaajien käyttö voi kuitenkin heikentää verkkoon syötetyn tehon laatua johtuen impedanssien yhteensopimattomuudesta. Tämä voi saada vaihtosuuntaajan tuottamaan harmonisia virtoja. Resonanssiongelmat voidaan analysoida ja ennaltaehkäistä käyttämällä teoreettista mallia vaihtosuuntaajan impedanssille tai mittaamalla sen taajuusvaste. Tässä diplomityössä käytetään pseudosatunnaisia binäärijaksoja ja verkkoemulaattoria vaihtosuuntajan ulostuloimpedanssin mittaamiseen laajalta taajuusalueelta.

Testeissä injektoidaan pseudosatunnaista signaalia verkkojännitteen referenssiin. Verkon jännitteet ja virrat mitataan ja niiden sisältämän informaation perusteella lasketaan vaihtosuuntaajan taajuusvaste. Mittaukset verifioidaan vertaamalla niitä passiivipiirien teoreettisiin arvoihin sekä testatusta invertteristä aikasemmin käytetyllä systeemillä saatuihin mittaustuloksiin.

Diplomityön metodia voidaan käyttää vaihtosuuntaajan impedanssimallien verifiointiin sekä vaihtosuuntaajan ohjauksen dynaamisen käyttäytymisen tutkimiseen. Tehdyt testit näyttävät, että metodi on suhteellisen tarkka suurella taajuusalueella, se on nopea ja helppo säätää vaadittujen mittausten mukaiseksi.

PREFACE

This Thesis has been done for the laboratory of Automation and Hydraulics and the laboratory of Electrical Energy Engineering at the Tampere University of Technology as a part of Academy of Finland research project. I would like to thank the university and the department for the opportunity to do my thesis.

I would like to thank my colleagues in the research project for the support and help given for finishing the thesis. I would like to thank Dr. Tomi Roinila and Dr. Tuomas Messo for giving insight on various theoretical and technical aspects of the work and for patience during the learning process with the project in hand.

Tampere, 8.3.2017

Tommi Reinikka

TABLE OF CONTENTS

LIST OF ABBREVIATIONS AND SYMBOLS

ABBREVIATIONS

AC	Alternating current
ADC	Analog to digital converter
DAQ	Data Acquisition
DAC	Digital to analog converter
DC	Direct current
DG	Distributed generation
dSPACE	Real-time simulator hardware and software producer
FFT	Fast fourier transform
FRF	Frequency response function
LHP	Left half-plane
MLBS	Maximum length binary signal
NI	National Instruments
PCC	Point of common coupling
PLL	Phase locked-loop
PV	Photovoltaic
PRBS	Pseudo-random binary signal
RHP	Right half-plane

SYMBOLS

a	MLBS amplitude
$\mathbf{A}$	System matrix
$\mathbf{B}$	Input matrix
$\mathbf{C}$	Output matrix
C	Capacitance
$\mathbf{D}$	Input-output matrix
d_{d}	direct component duty ratio
d_{q}	quadrature component duty ratio
f_{BW}	Bandwidth of the measurement
f_{g}	Grid frequency
f_{gen}	PRBS generation frequency

f_{res}	PRBS resolution
f_{s}	Sampling frequency
f_{var}	PRBS maximum allowed variance
G	Feedback loop gain transfer function
$G_{\mathrm{co\text{-}d}}$	Source-affected open-loop d-component control-to-output transfer function
$G_{\mathrm{co\text{-}q}}$	Source-affected open-loop q-component control-to-output transfer function
$G_{\mathrm{co\text{-}dq}}$	Source-affected open-loop cross-coupling control-to-output transfer function
$G_{\mathrm{co\text{-}qd}}$	Source-affected open-loop cross-coupling control-to-output transfer function
H	Open-loop transfer function of the system
i_{a}	Phase-a current
i_{b}	Phase-b current
i_{c}	Phase-c current
i_{in}	Input DC-current
i_{od}	Output current d-component
i_{oq}	Output current d-component
I_{S}	Source current
K_{p}	Controller proportional gain
K_{i}	Controller integral gain
$\mathbf{L}$	System transfer function
L	Inductance
N_{sin}	Number of grid voltage sequences
P	Length of MLBS period
R	Number of MLBS periods
s	Laplace variable
u	Input signal
u_{ek}	Input signal with noise
u_{a}	phase-a voltage
u_{b}	phase-b voltage
u_{c}	phase-c voltage
u_{d}	voltage d-component
u_{od}	output voltage d-component
u_{oq}	output voltage q-component
u_{q}	voltage q-component

u_0	voltage 0-component
V_{range}	Measurement voltage range
V_{res}	Measurement voltage resolution
X_{k}	Measured input signal
y	Output signal
$\mathbf{Y}$	Input matrix
Y_{k}	Measured output signal
y_{rk}	Output signal with noise
$Y_{\text{o-d}}$	D-component output admittance
$Y_{\text{o-q}}$	Q-component output admittance
Z_{L}	Load impedance
$Z_{\text{o-d}}$	D-component output impedance
$Z_{\text{o-q}}$	Q-component output impedance
Z_{S}	Source impedance
Φ_{MLBS}	Frequency Spectrum of the MLBS

1.   INTRODUCTION

Power electronics have become an important part of the power systems during the last couple of decades and continue to have more significant role in the future. This is due to better controllability, smaller size and cheaper production compared to older systems which use for example transformers for voltage conversion. Capability to easily convert DC power into AC and vice versa makes the use of power electronics appealing.

Renewable energy sources, such as solar and wind, and other distributed generation (DG) units require an efficient and controllable way to connect them to the grid. The best option is to use power electronics for connecting the DG unit to the grid. As DGs are becoming more common the effect of power electronic devices used in them is noticeable in the power grid. The systems have to be well designed as poor designing of the power electronic devices may cause power quality issues, complicated system design and make the systems harder to control [1].

Power electronic converters such as inverters are used to connect the DG-unit to the grid because of their capabilities to convert DC power into AC power and ability to synchronize the power generation to the grid frequency. However large amount of grid-connected converters introduce stability issues [2]. Inverters can cause large amount of harmonics and may turn unstable due to variation in grid impedance if not designed properly [3]. The requirements for DG-units are regulated through standards such as IEEE standard 1547 for Interconnecting Distributed Resources with Electric Power Systems [4].

Design of the control of the power electronics has to be tested and made with care because of the requirements of reliable operation and the ability to control power flow and power quality. The capabilities required by the grid standards for the DG units include active and reactive control, limits for harmonics and flicker, disconnecting from the power grid when needed for safety reasons and ride through of different grid faults before the malfunctioning part of the grid is disconnected [5]. All of these

requirements are becoming more strict as more and more DG units are connected to the grid.

Stability of an individual inverter can be determined by detailed inverter control models and analysis which is important for their design. However, when the goal is grid stability, the inverters external behavior is more interesting than its internal stability [6]. For grid stability evaluation impedance-based stability analysis is easier to apply than system models as it does not require exact internal system models for each inverter added to the system. Impedance based stability can be determined by comparing the inverter output impedance and grid impedance. The ratio between the impedances must satisfy Nyquist stability criterion for the system to be stable.

Evaluating the impedance-based stability margins requires accurate measurement of both inverter output impedance and grid impedance. Because the impedances change over time and with many parameters, online measurements are most desirable [7]. The measured sequence is a small-signal characteristic of the device which can be used to calculate its output impedance. The information is obtained by injecting small-signal perturbation on top of the nominal operating voltage. For measuring the inverter output impedance the perturbation has to be injected from the grid side and for measuring grid impedance it has to be injected through the inverter. The measurements can be used to validate stability of the system at the point of common coupling (PCC).

Pseudo-random binary signal (PRBS) is a commonly used perturbation signal for system identification. It has been successfully used for obtaining the grid impedance [8] - [10] and inverter output impedance [11] and is commonly used in system identification where disturbance to the normal operation has to be small [12]. Other perturbation signals used include injecting a controlled sine wave or use of a broadband injection such as impulse [13] and chirp signal [14]. The PRBS has favorable characteristics for impedance measurement compared to the other perturbation signals due to its low peak ratio, repeatability and ease of generation [15].

Power hardware-in-the-loop method for testing the inverter is favorable as it allows modifying the grid characteristics and inverter's controllers parameters online [11]. This can be implemented by using a dSPACE real-time simulator, current source emulator and a grid emulator. Inverter control and grid voltage references are simulated in real-time with dSPACE. Within the simulation perturbation signal can be injected to the voltage reference value and used for the measurement which allows

modeling of different grid dynamics and studying of grid-connected converters in time-varying conditions [2].

The problem in using a single dSPACE for simulating the whole system is that it causes the sampling frequency to be bound to the same frequency as the inverter control which makes the measurements slow. The inverter switching frequency is limited by need of blanking time between switching to avoid shorting the DC capacitor [2]. Separating the inverter switching frequency and grid voltage reference generation allows the use of higher sampling frequency and more accurate inverter output impedance measurements are obtained. However using another real-time simulator such as dSPACE is very expensive compared to the benefits gained from using separate control for the grid voltages.

In this thesis the grid voltage control is separated from the inverter and dSPACE. The reference voltages for the grid emulator are generated with much higher sampling frequency than the measurements done through the single real-time simulator which allows a high frequency generation of the PRBS signal. Characteristics of the inverter can be attained to a much higher frequencies than with the former measurement setup and the signal can be tuned to the required accuracy.

The rest of the thesis is organized as follows. Chapter 2 contains the theory of the inverter impedance-based stability, theory and advantages in using PRBS signal and the explanation of frequency response calculation. Chapter 3 presents the test system used in the thesis. Chapter 4 includes the tests of the system. In Chapter 5 the test results are analyzed and further improvements for the test system are proposed.

2. THEORY

This section of the thesis consists of the theory needed for implementing the perturbation signal and impedance based stability analysis of the inverter. Starting from the theory of evaluation system stability and ending in how to analyze the measurements acquired from the test. The theory of generation and the injection of the perturbation signal to the AC control reference are covered.

2.1   Impedance Based Stability

Weak grid characterized by high inductance is known to cause instability in grid-connected inverters. The impedance can destabilize the inverter current control loop and lead to sustained harmonic resonance or other instability problems. If the grid is stable without the inverter and the inverter is stable when the grid impedance is zero, the stability of the system can be determined from the ratio between output impedance of the grid-connected inverter and grid impedance. The inverter will remain stable if this ratio satisfies the Nyquist stability criterion [6].

Grid-connected inverters are operated as current sources and can be modeled by the Norton equivalent circuit. Fig 2.1 represents a basic grid-connected system. In the figure I_S is the grid-connected device presented as a current source, Z_S is the source impedance modeled parallel to the current source, V_L is the grid voltage which acts as the load of the system, Z_L is the grid impedance modeled in series with grid voltage. In this case the voltage across load which is the grid can be presented as

$$V(s) = I_S(s)Z_L(s) * \frac{1}{1 + Z_L(s)/Z_S(s)} \qquad (2.1)$$

This equation represents the interaction between the inverter and the grid. The variables of the system in the equation can be presented as a Thevenin equivalent circuit as shown in Fig. 2.1. This is the level of detail the inverter and the grid has

to be presented to perform the impedance based stability analysis
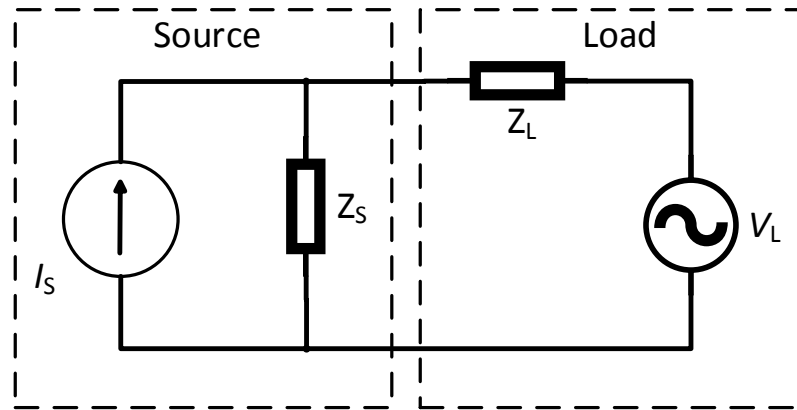

Figure *2.1* *Source load interaction of the grid and the inverter*

According to [6] it can be seen that for a current source system the output impedance should be high and ideally infinite. This causes the voltage $V(s)$ in Fig. 2.1 to be dependant only on the source current and load impedance. Fig. 2.2 presents the value of the grid impedance and two inverter models on a Bode plot. The figure presents an example of a stable inverter and unstable inverter.
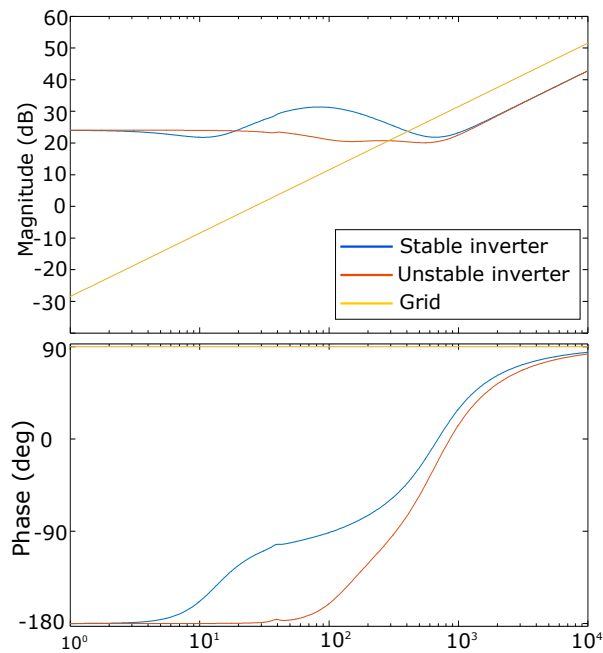
Figure ***2.2*** *Example bode diagram of grid impedance and two different inverter output impedances with stable and unstable control*

The inverter presented by the blue line in Fig 2.2 is stable but the inverter marked by the orange line is not. The stability can be interpreted from the crossover point of the inverter and grid impedances. The inverter presented by the orange line is not stable as it has over 180 degrees phase-shift at the frequency where inverter and grid impedance have the same magnitude. The output impedance of the inverter is affected by its own performance, output filter design and grid-synchronization method. The effect of these have been studied in [16] and [17]. Shaping of the output impedance can be done by choosing the right control parameters.

Frequency domain stability can be investigated by using Nyquist stability criterion. Technique created for evaluating stability of linear control systems by Harry Nyquist in 1932. The method is based on theory of the function of a complex variable due to Cauchy theorem. It is concerned with mapping contours in the complex s-plane.[18]

The relative closed-loop stability is determined by examining the characteristic equation of the system

$$F(s) = 1 + L(s) = 0, \tag{2.2}$$

where $L(s)$ is the system transfer function and for single loop control system it is $L(s) = G(s)H(s)$, where $G(s)$ is the feedback loop gain transfer function and $H(s)$ is the open-loop transfer function for the system. The method can be used for both single and multi-loop systems.

Basis for this criterion is that the system is stable if and only if the countour in the $L(s)$ plane does not encircle the (-1,0) point when the number of right-half-plane zeros is zero. If there are more than 0 poles in the right half plane the system is stable only and only if the the point (-1,0) is encircled counterclockwise equal times to the number of right half plane (RHP) poles [18]. The Nyquist diagram which is used to interpret the results can be seen in Fig. 2.3 which shows a Nyquist plot of two different systems. The figure can be used to predict stability or unstability of the system by seeing whether the drawn line encircles the point (-1,0). In a system where all of the poles of the transfer function are on the left half-plane (LHP) the system is stable if the contour does not encircle the point (-1,0) clockwise and unstable if the contour encircles that point clockwise.

For most of the systems it is easy to ensure their stability by determining that they have no RHP poles [18]. Using Nyquist plot to for determining guaranteed system stability has been studied in [19]. The research is done to find forbidden zones for the contour. When the contour does not enter these zones the stability of the system is guaranteed.

Fig. 2.3 is shows an example of an unstable and a stable system. The Nyquist diagram for defining inverter stability can be drawn similarly to Fig. 2.3 from the inverter output impedance and grid impedance ratio $Z_{\mathrm{L}}(s)/Z_{\mathrm{S}}(s)$.
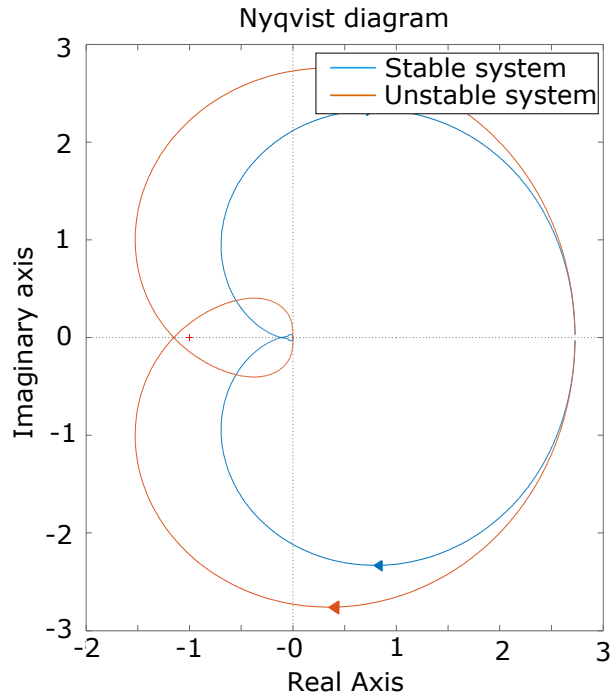
Figure *2.3 Example of Nyquist diagram of a stable and unstable system*

Closed-loop system gain and phase margins can be seen from the diagram in addition to the system stability. Gain and phase margins are easier to evaluate from a Bode diagram so it is more preferable to draw a Bode diagram than a polar plot. The crossing from a stable system to a marginally stable system occurs at point $-1 + j0$ in $L(s)$ which is equivalent to a logarithmic magnitude of $0dB$ and a phase angle of 180 or -180 on a Bode plot [18]. Complete Nyquist plot should still be used to determine stability.

2.2   PRBS Perturbation Signal

Important part of online system identification for practical use is that the system perturbation should not disturb the system in terms of static and dynamic voltage regulation. Switching and quantization noise should not affect the identification. Memory and processing requirements of the measurement should be low [20]. These requirement can be fulfilled by using Pseudo Random Binary Signal (PRBS) as the perturbation signal.

The PRBS is one of the commonly used perturbation signals for system identification. This is due to its good properties as a test signal and ease of generation. The PRBS has these properties because it resembles white noise but the signal is binary and has a predetermined sequence due to its implementation design. The predetermined sequence allows repeating of the sequence allowing effective noise cancelation from the measurements with the use of averaging.

Properties of the PRBS include [15]

- The signal has only 2 levels which can change from one level to the other only during certain event points (0,t,2t,...).

- The level of the signal at certain point is predetermined and is always the same. PRBS is deterministic and repeatable.

- The PRBS is periodic with period $T = N\Delta t$, where N is an odd integer

- In any period, there are $1/2(N + 1)$ intervals where the signal is at one level and $1/2(N - 1)$ interval where it is at the other

A feedback shift register can be used for generating the PRBS signal. The output is the last bit of the in the register sequence and the new input value is generated from the current state of the register. The input can be calculated as a modulo-2 sum or XOR gate of the logic value of the last stage and one or more other stages [15]. The new input in to the register by this addition is given by $1 + 1 = 0 + 0 = 0$ and $1 + 0 = 0 + 1 = 1$. By choosing carefully the structure of the feedback register and location(s) of the feedback loop(s) the length of the signal is $2^n - 1$. This is called Maximum length binary signal (MLBS). 4-bit shift register is presented in Fig. 2.4.
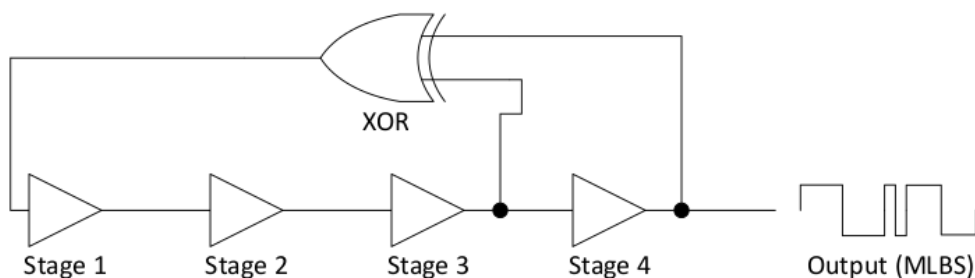

Figure 2.4 *4 stage shift register*

With the 4-bit register shown in Fig. 2.4 a sequence with $2^4 - 1$ different states can be generated. One possible sequence of the 4-bit PRBS signal is presented in Table 2.1.

Table **2.1** *Maximum length binary sequence from a four-stage shift register*

State number	Shift	register	stage		output
	(1)	2	3	4	
1	0	0	0	1	1
2	1	0	0	0	0
3	0	1	0	0	0
4	0	0	1	0	0
5	1	0	0	1	1
6	1	1	0	0	0
7	0	1	1	0	0
8	1	0	1	1	1
9	0	1	0	1	1
10	1	0	1	0	0
11	1	1	0	1	1
12	1	1	1	0	0
13	1	1	1	1	1
14	0	1	1	1	1
15	0	0	1	1	1
16	0	0	0	1	1

The starting sequence can be freely chosen but it cannot have all values set to 0. This causes the register to never changes its value. The amount of different states the register has depends on the layout and only few of the possible feedback connections produce the maximum length binary sequence (MLBS) with length of $2^n - 1$. Register with the maximum length has a characteristic equation in the delays in the register, which corresponds to a primitive polynomial, modulo 2 [15].

Fig. 2.5 shows time and frequency domain waveforms of a PRBS which was generated with a sampling frequency 4 times greater than the PRBS generation frequency. The power spectrum of the PRBS signal can be seen from the frequency domain waveform. Energy spread of the PRBS is not uniform over the whole bandwidth and decreases to zero at the generation frequency.
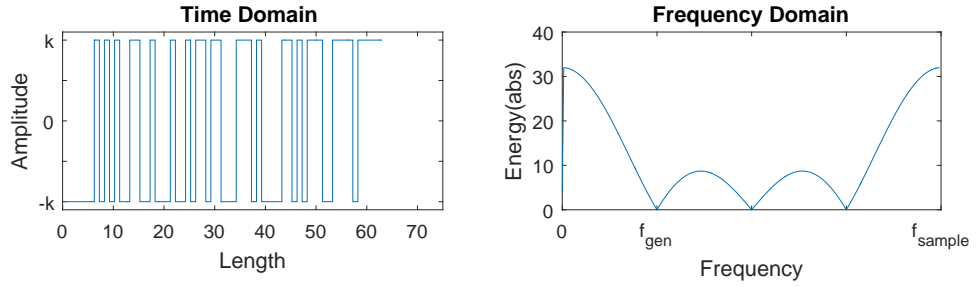
Figure 2.5 *PRBS generated with 4 bits with amplitude k and generation frequency f_{gen}*

The generation frequency f_{gen} should be chosen so that the excitation has enough energy for required bandwidth. The spectrum Φ_{MLBS} is considered flat until the power has dropped to $|\Phi_{\text{MLBS}} f_1|/\sqrt{2}$ which is about -3 dB [21]. The chosen generation frequency f_{gen} should be around 2.5 times the maximum frequency of interest [15].

The PRBS has the advantage of being faster and having lower peak ratio compared to other perturbation signals. This allows it to be used on system that are delicate and cannot sustain high-amplitude perturbations [15].

Other perturbation signals used for system identification are impulse, sine wave, multisine signal and random noise. In this thesis sine wave is used for measuring the reference value as it is accurate and time is not an issue during experimental tests. The use of pseudo-random binary signal and other multilevel perturbation signals will reduce the time needed for the system identification by a huge margin as it excites all of the desired frequencies at once and sine wave excites the system only at one certain frequency at a time. With sine wave it is needed to wait for the transients of the system to disappear until it can be measured reliably. The process is then repeated again for all of the frequencies needed for the testing [15]. The measuring process can last for a long time when measuring complex systems if the results are needed from wide bandwidth and small frequency resolution.

Multifrequency excitation can be done for example with impulse, multisine and random noise signal. Impulse response requires high amounts of energy to the impulse for the frequency response analysis [13]. Multisine and random noise are hard to implement as both of the signals have an infinite amount of different signal levels in an ideal case. Multisine has a high peak factor when high frequencies are needed for

the system response. This can cause damage to the tested system or cause distortion in the results due to saturation effects. Random noise is susceptible to noise and spectral leakage. As the length of the PRBS signal is periodic there is no need for windowing as with many other multifrequency signals. [15]

The PRBS signal allows the perturbation to be generated with ease but some things needs to be taken into account when it is used. The PRBS signal generated maximum length binary sequence (MLBS) has a set length of $2^n - 1$. The test signal has to be multiple of integers of this length [15]. The spectrum of signal is flat and cannot be arbitrary chosen. This means that single frequencies have low amount of power and are susceptible to noise. The system which is tested needs to be linear as nonlinearities cannot be determined with PRBS signal [22].

2.2.1   Generation of a MLBS Perturbation Signal

The MLBS perturbation has several characteristics to be considered in the design procedure. The specification variables includes the required bandwidth (f_{BW}), required frequency resolution (f_{res}) and maximum allowable variance of the frequency response function (FRF) (f_{var}). The following are the design variables of the system: MLBS generation frequency (f_{gen}), length of the one MLBS period (P), Number of MLBS periods (R) and MLBS amplitude (a) [21].

The generated signal can defined both as a discrete and continuous signal which both have different shapes [21]. This can result in significant error when Fourier transformation is applied since it has equal amplitude shape of the transformed function. To avoid the incorrect shape caused by discrete signal sampling of the signal, multisampling has to be used. The effect of multisampling is known as aliasing. Using two samples for one bit of the MLBS signal reduces the error significantly [21]. The upper limit of the possible bandwidth in frequency response analysis is determined by this. Maximum bandwidth is half of the sampling frequency and this frequency is known as Nyquist frequency.

To obtain the required bandwidth of the measurement the generation frequency (f_{gen}) of the PRBS signal has to be 2.5 times greater than f_{BW}. Since the measurements from the system are done with the same sampling frequency as the signal generation aliasing has to be taken into account when determining the bandwidth of the measurement. This means that the sampling frequency (f_s) of the measurements

and signal generation has to be

$$f_{\mathrm{s}} = f_{\mathrm{BW}} * 2.5 * 2 = 5 * f_{\mathrm{BW}} \tag{2.3}$$

2.2.2   Resolution

The PRBS signal has its energy at certain frequencies varying from 0 to the generation frequency. Each of the frequencies presents in signal are at certain interval from each other. Length of this interval is the resolution of the measurement. It is dependent on the generation frequency of the PRBS and the number of bits in the PRBS. The resolution can be calculated as follows

$$f_{\mathrm{res}} = \frac{f_{\mathrm{gen}}}{N} \tag{2.4}$$

where f_{res} is the frequency resolution. When applying the PRBS to a system analysis the resolution has to be accurate enough to satisfy the needs of the measurement at all frequency levels. The generation frequency is used to set the bandwidth of the measurement to the required range and the length of the PRBS is used to provide the needed resolution.

2.3   Fourier Methods

Frequency response of the system can be calculated from its input and output signals. The perturbation signal $x(t)$ is the input going into the system which results in an output response $y(t)$.
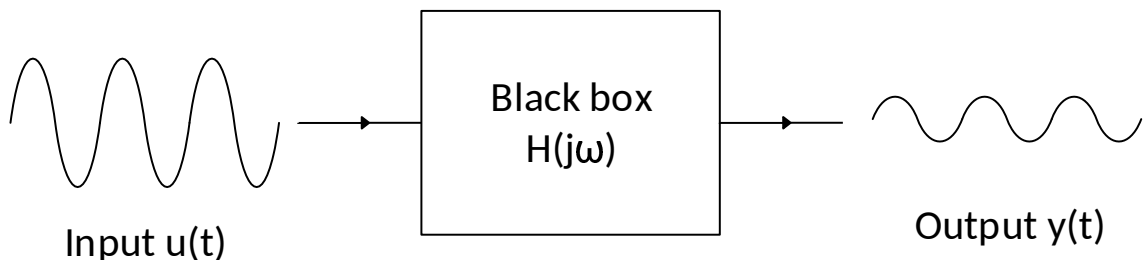

Input u(t)   Black box H(jω)   Output y(t)

Figure 2.6 Black box system

Fig. 2.6 shows the idea of how frequency response is determined. The sinusoidal signal injected into a linear system produces an ouput signal at the same frequency as the input. The phase and magnitude of the signal can however change from the input. Their difference to the original signal is a function of the input signal [18]. We are interested in the steady-state response of the system at different frequencies.

When transformed to frequency domain with fourier transformation the measured input and output signals can be used to calculate the frequency response function of the system. This can be computed with Fast Fourier Transformation (FFT) algorithm. The frequency response can be calculated with the following equation

$$G(j\omega) = \frac{y(j\omega)}{u(j\omega)}, \tag{2.5}$$

where $y(j\omega)$ and $u(j\omega)$ are frequency domain transformed versions of the input $u(t)$ and output $y(t)$ signals. However, both of these signal are affected by noise which causes the frequency response waveform to not follow the real value. The disturbance caused by the noise can be decreased by repeating the PRBS test sequence several times and averaging the results. As the noise does not correlate with the output or the input signals the frequency response function (FRF) can obtained by averaging the results [8]. There are few different methods of doing the averaging. Logarithmic averaging works effectively and can be done as

$$G_{\log}(j\omega) = \left(\prod_{k=1}^{R} \frac{y_{\mathrm{rk}}(j\omega)}{u_{\mathrm{ek}}(j\omega)} \right)^{1/P}, \tag{2.6}$$

where y_{rk} and u_{ek} are the frequency domain transformed input and output signals which include noise. Logarithmic averaging gives accurate results with the gain value of the frequency response but it cannot be used for the phase as imaginary values do not keep their angles when multiplied. Another way to calculate the averaged frequency response is to use the spectrum method [15]. In this method the data is first transformed into frequency domain and the averaging is done by means of cross-spectrum between the input and output spectra. This method avoids phase wrapping and gives unbiased estimate of the phase but is less accurate than the logarithmic averaging method. When using the spectrum method either input or output noise can be suppressed depending on the values used [15]. Averaging with

the spectrum method is done in frequency-domain. The measured output and input signals are first transformed into frequency domain and then correlation equations are then averaged. The spectrum method for averaging can be done as follows

$$G_1(j\omega) = \frac{\frac{1}{N}\sum_{k=1}^{N} Y_k(j\omega) * X_k^*(j\omega)}{\frac{1}{N}\sum_{k=1}^{N} X_k(j\omega) * X_k^*(j\omega)},\qquad(2.7)$$

where $G_1(j\omega)$ is the transfer function between the measured signals, $Y_k(j\omega)$ is the measured output signal and $X_k(j\omega)$ is the measured input signal. In(2.7) the spectrum method is used to remove the noise from the input values. For removing the noise from the output values of the following transfer function is used

$$G_2(j\omega) = \frac{\frac{1}{N}\sum_{k=1}^{N} Y_k(j\omega) * Y_k^*(j\omega)}{\frac{1}{N}\sum_{k=1}^{N} X_k(j\omega) * Y_k^*(j\omega)},\qquad(2.8)$$

where $G_{2(j\omega)}$ is the transfer function between the measured signals. Noise can be removed from either input or output but not both when using the spectrum method for averaging [15].

2.4 DQ-Transformation

The voltage and current values and measurements used in the experiment for analyzing the inverter are transformed into DC-form as non-stationary values are problematic for the control and steady-state calculation. This can be done by transforming the variables into direct-quadrature plane with Parks transformation. Parks transformation changes the three phase-vectors into two vectors and then matches these two rotating vectors into rotating coordinates. Combining these two transformations results in the following formula which is known as Clarke's transformation

$$\begin{bmatrix} u_\mathrm{d}(t) \\ u_\mathrm{q}(t) \\ u_0(t) \end{bmatrix} = \frac{2}{3} \begin{bmatrix} \cos(\omega t) & \cos(\omega t - \frac{2*\pi}{3}) & \cos(\omega t - \frac{4*\pi}{3}) \\ \sin(\omega t) & -\sin(\omega t - \frac{2*\pi}{3}) & -\sin(\omega t - \frac{4*\pi}{3}) \\ \frac{1}{2} & \frac{1}{2} & \frac{1}{2} \end{bmatrix} \begin{bmatrix} u_\mathrm{a}(t) \\ u_\mathrm{b}(t) \\ u_\mathrm{c}(t) \end{bmatrix}\qquad(2.9)$$

where $u_\mathrm{d}(t)$ is the AC-voltage d-component, $u_\mathrm{q}(t)$ is the AC-voltage q-component, $u_0(t)$ is the AC-voltage zero-component, $u_\mathrm{a}(t)$, $u_\mathrm{b}(t)$ and $u_\mathrm{c}(t)$ are the a, b and c

phases of the three-phase grid voltages. This forms a DC-value from the AC voltage and current waveforms. Advantage of this is that the system can be controlled using DC values instead of AC which allows to use basic PI-controllers. The equation is amplitude invariant which means that the voltage of the d-component is equal to amplitude of phase voltage in a balanced three-phase system if the q-component is zero.

The same transformation can be done to the opposite direction. DC in dq-plane values are transformed into the AC values by

$$
\begin{bmatrix} u_\mathrm{a}(t) \\ u_\mathrm{b}(t) \\ u_\mathrm{c}(t) \end{bmatrix} = \frac{2}{3} \begin{bmatrix} \cos(\omega t) & \sin(\omega t) & 1 \\ \cos(\omega t - \frac{2*\pi}{3}) & \sin(\omega t - \frac{2*\pi}{3}) & 1 \\ \cos(\omega t + \frac{4*\pi}{3}) & -\sin(\omega t - \frac{4*\pi}{3}) & 1 \end{bmatrix} \begin{bmatrix} u_\mathrm{d}(t) \\ u_\mathrm{q}(t) \\ u_0(t) \end{bmatrix} \tag{2.10}
$$

The injection of the PRBS signal can be done in dq-plane and then transformed into AC values for actual use. The effect of the perturbation signal persists in the transformation. Frequency response analysis can be done by transforming the measured values into dq-domain.

The measured inverter system is non-linear. In order to apply modeling and control techniques used for the linear systems the inverter has to be near its operating point when the measurements are made [23].

2.5   Small Signal Model

Inverters can be modeled as a series of equations which are the transfer functions between their inputs and outputs. These equations can be formed if all of the components in the inverter and its layout is known. However these calculations become increasingly difficult when more components or additional control schemes are added into the system. These include for example input and output filters, power source with nonfinite output impedance, additional output voltage levels and phase-locked loop or voltage-feedforward control loops. The small-signal model means that the system is linearized at a certain operating point and all of the transfer functions used in the model are only valid near that certain point.

One of the most common methods to attain the small signal model of a three-phase inverter is to transform all of the three-phase signals into DC values by using a

synchronous reference frame rotating at the same angular frequency as the three-phase grid. This is done by using (2.9). The dq-domain is used for the three-phase voltages and currents because they are easier to use for calculating the steady-state operating point. Measuring the impedances in dq-domain is straightforward [24].
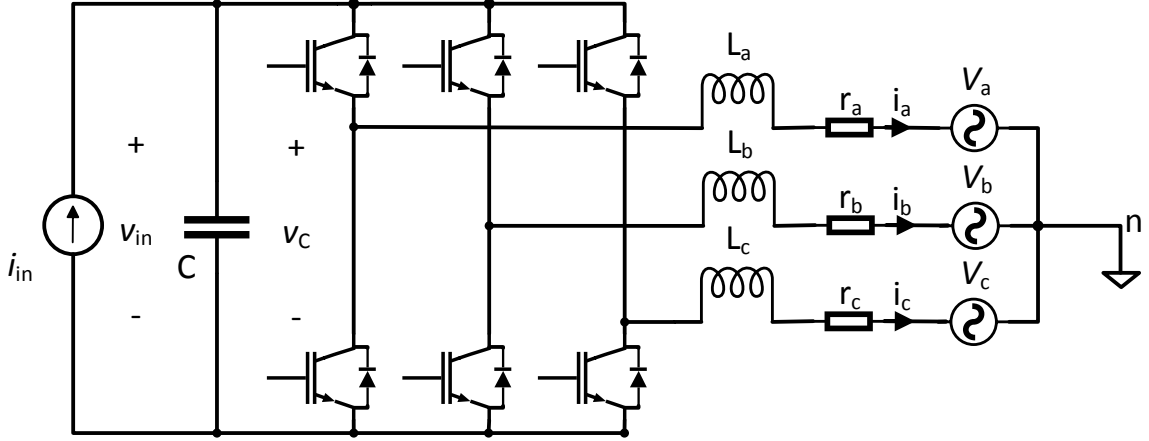

Figure *2.7 Simple inverter power stage*

The layout of a basic inverter is presented in Fig. 2.7. A current source is feeding the 2-level inverter with switches and L-filter in the output. System inputs are the DC-current i_{in} and the three-phase voltages v_a, v_b and v_c and the output are the three-phase currents i_a, i_b, i_c and the DC-voltage v_{in}. Input values are controlled by the source and the load of the system. In this thesis the source is a photovoltaic (PV) emulator and the load is a grid-emulator.

The model is created by forming the voltage and current equations for all of the outputs and state variable within the system in both on and off states of the switches. The state variables are all the capacitors voltage and inductor currents presented in the system. These equations are then transformed into dq-coordinates. Next step is to use these equations to find out the steady state operating point for all of the variables present in the system based on the known operating point. The average values of the variables in the set operating point are calculated by setting all of the derivatives to zero and using the known values in the equation. The known values in this model are the input values of the system and the DC-side voltage as the power generated is assumed to be known and determined by the PV-generator not the inverter.

The average model equations are non-linear due to multiplication of duty ratios with other variables. Due to non-linearity of the equations the model has to be linearized. The average values derived in the previous step for the set operating point are used for this. The linearization is done by calculating partial derivatives for the all state, input and output variables [16]. The linearized equations are then presented as state-space model

$$\begin{bmatrix} d\hat{\mathbf{x}}(t) \\ \hat{\mathbf{y}}(t) \end{bmatrix} = \frac{2}{3} \begin{bmatrix} \mathbf{A}\hat{\mathbf{x}}(t) & \mathbf{B}\hat{\mathbf{u}}(t) \\ \mathbf{C}\hat{\mathbf{u}}(t) & \mathbf{D}\hat{\mathbf{u}}(t) \end{bmatrix}, \tag{2.11}$$

where $\hat{\mathbf{x}}$ are the state variables, $\hat{\mathbf{u}}$ are the input values, $\hat{\mathbf{y}}$ are the output values and matrices $\mathbf{A}$, $\mathbf{B}$, $\mathbf{C}$ and $\mathbf{D}$ are the constant values calculated in the linearization of the equation. These values can be Laplace-transformed as the equations are linearized. the Laplace domain values can be used solve the transfer function matrix $\mathbf{G}$ between the input and output variables. The equation to for the transfer function is as follows

$$\mathbf{Y}(s) = [\mathbf{C}(s\mathbf{I} - \mathbf{A})^{-1}\mathbf{B} + \mathbf{D}]\mathbf{U}(s) = \mathbf{G}\mathbf{U} \tag{2.12}$$

The transfer function in (2.12) is composed of different transfer functions between each input and output of the system at the given operating point. The matrix of transfer functions can be presented as given in dissertation [17].

$$\begin{bmatrix} \hat{u}_{\text{in}} \\ \hat{i}_{\text{od}} \\ \hat{i}_{\text{oq}} \end{bmatrix} = \begin{bmatrix} Z_{\text{in}} & T_{\text{oi-d}} & T_{\text{oi-q}} & G_{\text{ci-d}} & G_{\text{ci-q}} \\ G_{\text{io-d}} & -Y_{\text{o-d}} & -Y_{\text{o-qd}} & G_{\text{co-d}} & G_{\text{co-qd}} \\ G_{\text{io-q}} & -Y_{\text{o-dq}} & -Y_{\text{o-q}} & G_{\text{co-dq}} & G_{\text{co-q}} \end{bmatrix} \begin{bmatrix} \hat{i}_{\text{in}} \\ \hat{u}_{\text{od}} \\ \hat{u}_{\text{oq}} \\ \hat{d}_{\text{d}} \\ \hat{d}_{\text{q}} \end{bmatrix} \tag{2.13}$$

The transfer functions in (2.13) describe how each of the input of the system affect the outputs. The stability and control of the system can be modified by choosing the transfer function for controlled input-output variable interaction and modifying values in the transfer function such as gains, zeros and poles. For the control of the device the most important ones are transfer functions between control and output $G_{\text{co-d}}$ and $G_{\text{co-q}}$ and their cross-couplings $G_{\text{co-qd}}$ and $G_{\text{co-dq}}$. Modifying these values allows to change the speed and the stability margins of the control. The control

block diagram for the output currents $\hat{i}_{\text{o-d}}$ and $\hat{i}_{\text{o-q}}$ can be presented as in Fig. 2.8.
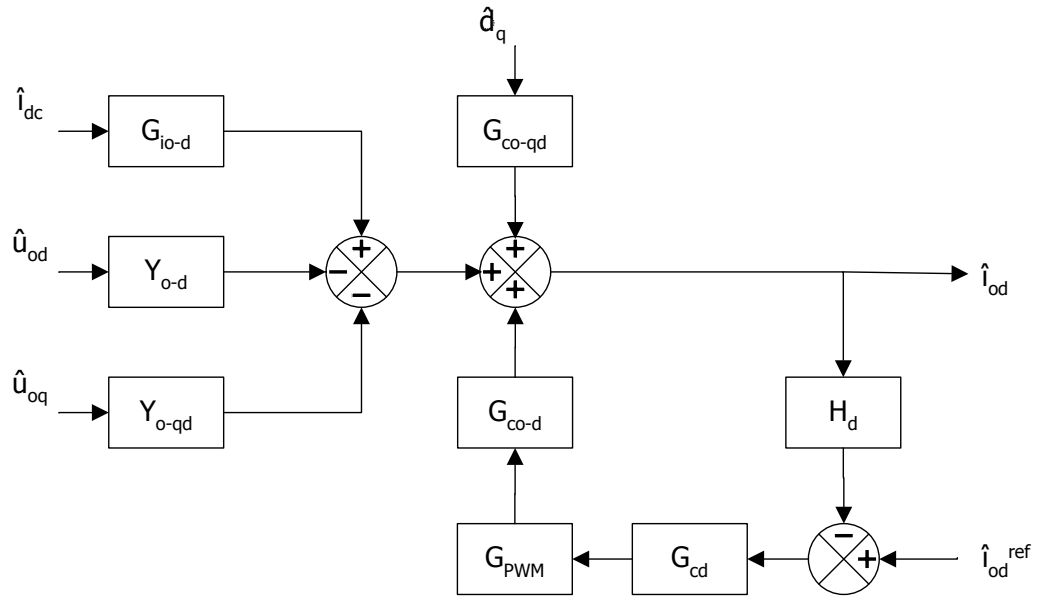
(a) id control block-diagram
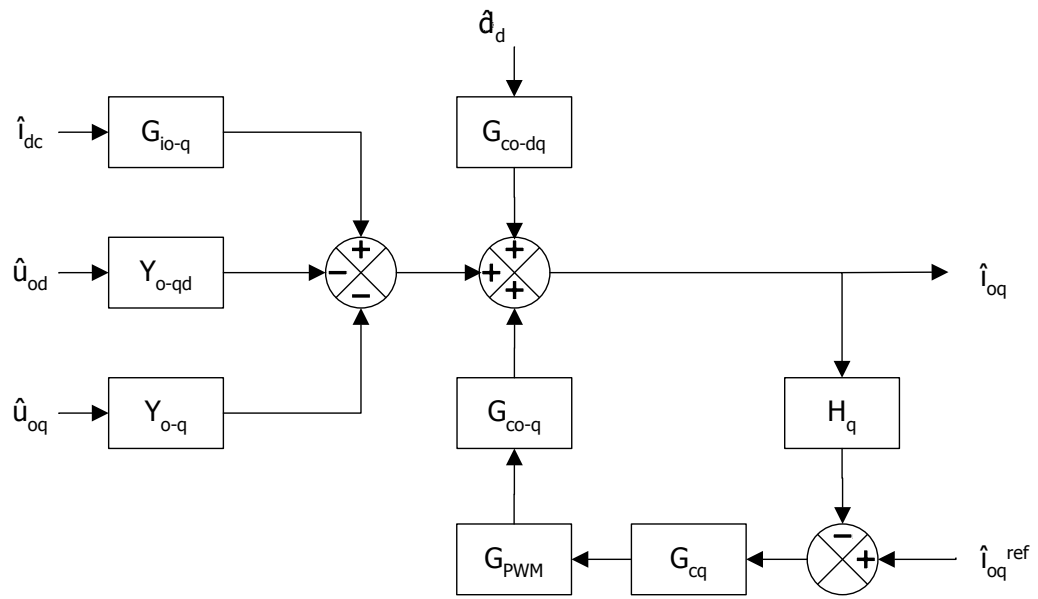
(b) iq control block-diagram

***Figure* 2.8** *Control block diagram of the inverter output current*

The control block diagrams in 2.8 is an example of the factors affecting the output current in an inverter. It does not include DC-voltage control, PLL or voltage

feedforward which are common in inverter control scheme. The control block diagram becomes increasingly difficult to form as the model is made more accurate by adding different forms of control, filtering and source and load interactions into the equations. Theoretical models of inverters with additional parts of the system and control have been studied in other works and are not part of this thesis. The source and the load affected model of a PV inverter with an LCL-filter is studied in [25], the effect of voltage boosting DC-DC converter on DC-link control and effect phase-locked loop and voltage feedforward on inverter control have been studied in [17].

For the purpose of this thesis and the output impedance measurement we are interested in the output impedances $Z_{o\text{-}d}$, $Z_{o\text{-}q}$ and the cross-connection of the d and q domains $Z_{o\text{-}dq}$ and $Z_{o\text{-}qd}$ which are interchangeable with the admittance values $Y_{o\text{-}d}$, $Y_{o\text{-}q}$, $Y_{o\text{-}dq}$ and $Y_{o\text{-}qd}$ presented in (2.13). The output impedance values will be measured with frequency response method up to multiple kilohertz range. This allows validation of mathematical models of the inverter to higher frequencies and further development of the models.

3.   EXPERIMENTS

3.1   Experimental Setup

The goal of the test setup is to measure the output impedance of the inverter by injecting a PRBS-signal into the grid voltage which is the output voltage of the inverter. Both the inverter grid voltage and the output current are measured. Frequency response is calculated from the measurements while the system is online. The output impedance can be seen from the bode plot as the frequency response between the output voltage and current.

3.2   Layout of the Test System

Experimental setup consists of a grid emulator, inverter and PV-simulator. The control signal for the grid emulator is produced by NIDAQ-6363 data acquisition card (DAQ). Inverter output voltages and currents are measured with the voltage and current probes. The measurement devices are connected to the DAQ-device. The data acquired is processed in Matlab to produce the frequency response while system is online. The layout of the measurement setup used in the experiments is presented in Fig. 3.1. The setup consists of a photovoltaic-emulator (PV-emulator), inverter, grid emulator, dSPACE real-time simulator controlling the PV-emulator and the inverter, DAQ measurement card control the grid and a PC connected to the dSPACE and the DAQ-device. The simulations are done and operated with Matlab.
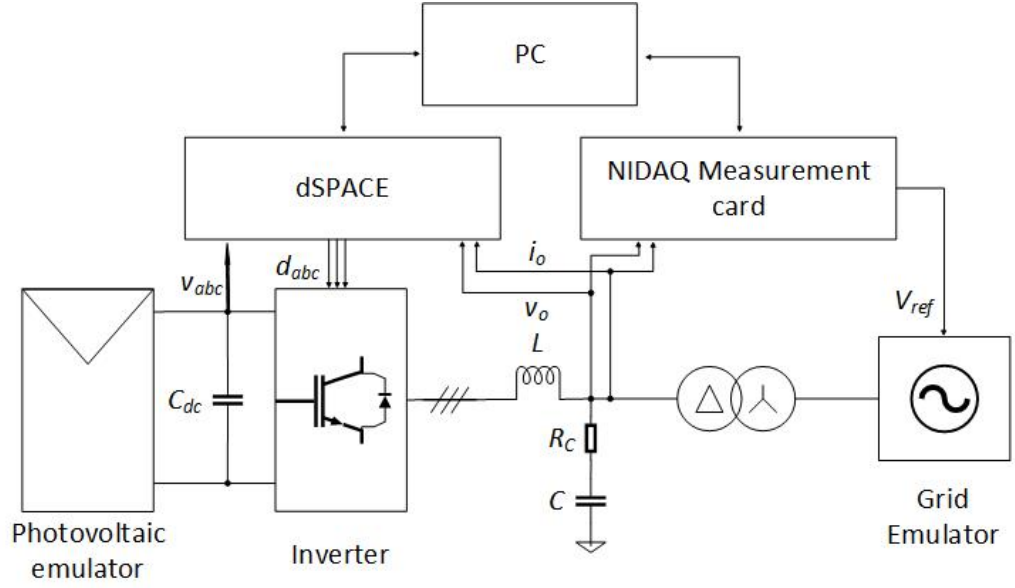
***Figure 3.1** Block diagram of the system discussed in the thesis*

There are two voltage probes and two current probes which are used for the measurements. These values can be used to calculate phase voltage and currents for all three phases. The measured voltages are main voltages and line-to-neutral values can be calculated with the following set of equations when the system is symmetrical.

$$v_{ab} = v_a - v_b \tag{3.1}$$

$$v_{bc} = v_b - v_c \tag{3.2}$$

$$v_{ca} = v_c - v_a \tag{3.3}$$

$$v_a + v_b + v_c = 0 \tag{3.4}$$

The equations for each phase voltage are the following

$$v_a = -\frac{1}{3} * v_{ab} - \frac{2}{3} * v_{ca} \tag{3.5}$$

$$v_b = -\frac{2}{3} * v_{ab} - \frac{1}{3} * v_{ca} \tag{3.6}$$

$$v_c = -v_a - v_b \tag{3.7}$$

The equations hold true when the system is symmetrical as all the phase voltages summed together equals zero. The two current measurements can be used the same way as the total current according to the Kirchhoff's law is zero

$$i_a + i_b + i_c = 0 \tag{3.8}$$

$$i_c = -i_a - i_b \tag{3.9}$$

The equation is true when the system is symmetrical and there is no neutral line.

3.3 Measurement Unit (NI-DAQ USB-6363)

The measurement unit used for the control of the grid emulator and to read measurements from the measurement probes is NI-DAQ USB 6363 data acquisition card produced by National Instruments. The device is shown in Fig. 3.2

Figure 3.2 NI-DAQ USB 6363 data acquisition card

The DAQ-device has 16 analog inputs and 4 analog outputs which is enough to

implement the impedance measurement setup. The required amount of connections are 4 input channels and 3 output channels. Required inputs are for 2 phase voltages and 2 phase currents. The outputs needed for the system are for sending the reference values of each phase voltage to the grid emulator. The essential data specifications of the used DAQ-device are shown in Table 3.1

Table 3.1 *Essential NI-DAQ USB-6363 data specifications*

Number of input channels	16 differential
Number of output channels	4
ADC and DAC resolution	16 bits
Timing resolution	10 ns
Input range	± 0.1 V, ± 0.2 V, ± 0.5 V, ± 1 V, ± 2 V, ± 5 V, ± 10 V,
Output range	± 10 V, ± 5 V
Maximum multichannel input sample rate	1.00 MS/s (aggregated)
Maximum simultaneous 3 channel output update rate	1.54 MS/s

The DAQ-card allows sampling frequency to be up to 1 Mhz per channel. The output channels of the device change their values simultaneously. This means that each of the voltage control values sent to the grid emulator change at the same time and there is no error in control caused by the speed of the device. However the input connectors share the same channel in the device. Sharing of the same channel for all of the input connectors means that the maximum possible sampling frequency for the input channel is 1 MHz divided by the number of inputs used on the device. For this implementation this reduces the maximum sampling frequency down to 250 kHz. Due to sharing of the input channel the values measured from the system are not taken at the exact same moment. One connector is measured at a time and saved into the memory of the DAQ-device in the order the values are taken. As the values of the input channels are not measured at the same time the measurements cause the signal to be out of phase when compared. This causes error to the measured phase of the impedance when determining frequency response analysis. This has to be taken into account when using the DAQ-device for setups and experiments which are sensitive to the information about the phase.

The resolution of the measurement device has to be taken into account when the measurements need to be accurate on a large range. The resolution of the measurement is defined by the DAC resolution and the input range and can cause quantization error if the measured difference is smaller than the resolution of the device.

The control of the NI-DAQ USB-6363 and other similar devices can be done using Matlab without much of programming experience. The control is done by using Matlab Data Acquisition Toolbox. Matlab was chosen as it is used to communicate with other devices used in the laboratory and to perform calculation needed for experiment setup. Other option would have been to use Labview which has greater support for devices produced by National Instruments but is not as simple as Matlab for performing mathematical operations. For better control over the device C-code could be used.

3.4 Grid Emulator

The inverter and the PV-simulator are connected to a grid emulator functioning as a load for system. The grid emulator is Spitzenberger & Spies PAS 15000 Grid emulator. It is composed of three 4-quadrant linear amplifiers, controller unit and an oscilloscope. The device repeats the reference voltages sent by NI-DAQ card.

The grid emulator is shown in Fig. 3.3. The device can operate both as a sink and a source. In this experiment the grid emulator is used as sink and no load resistors are needed to dissipate the energy going through the inverter. This means that there are no resistors to dampen the interactions between the inverter and the grid.

Figure 3.3 *Spitzenberger & Spies PAS 15000 Grid Emulator*

The manufacturer of the grid emulator promises bandwidth of 30 kHz for large-signals and 50 kHz for small-signals. The signal gets through the emulator with higher frequencies but suffers from dampening caused by the emulator as it cannot reproduce the control signal at frequencies over 30 kHz.

The frequency response of the emulator was measured. This can be used to estimate the effect of the grid emulator to its output signal. The test was carried by using 16-bit PRBS signal with generation frequencies of 100 kHz, 150 kHz and 250 kHz. The frequency response is calculated by comparing the calculated PRBS signal from Matlab and the measured output voltage of the grid emulator over $32,3\,\Omega$ resistance.
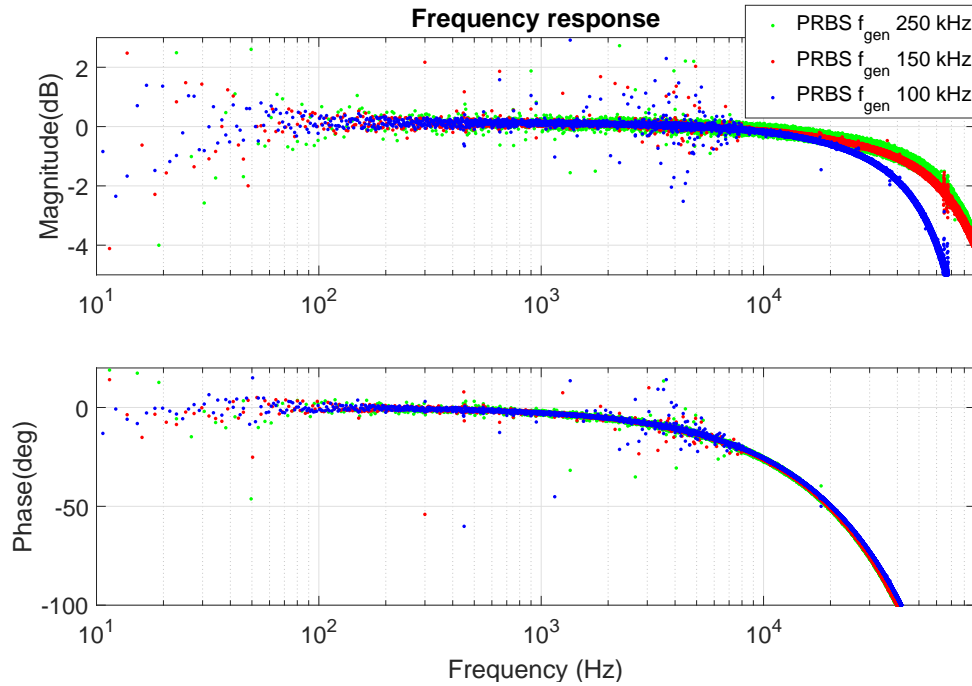
Figure 3.4 *Frequency response of the grid emulator*

Fig. 3.4 shows that the gain of the 150 kHz and 250 kHz signals have almost exactly the same frequency responses with the exception that the 250 kHz PRBS signal has significantly more noise in it. With the lower generation frequency of 100 kHz the measurements are no longer limited by the grid emulator and the limits are determined by the generation frequency of the PRBS signal. With 100 kHz signal the frequency response begins to deviate from the 0 dB gain at lower frequencies than with the higher PRBS generation frequencies. Both 150 kHz and 250 kHz signals cross the -3 dB point which means that the energy is halved at 75 kHz and have around -1.5 dB gain at 50 Khz. There is a delay in the signal going through the emulator and this causes the phase shift. However this is not significant for the experiment as the variable used for the comparison is not the control reference but the measured output voltage of the emulator. Any delay caused by the emulation is already in both input and output values used for frequency response analysis.

The frequency response made with the PRBS has enough energy to make accurate frequency response analysis up to 1/2.5 of its generation frequency. This means that while the emulator is unable reproduce the exact waveform of the PRBS signal it retains the correct information up to 50 kHz. This allows the use of higher frequency

PRBS than the bandwidth of the grid emulator.

3.5 Synchronising the PRBS and Voltage Reference

The PRBS signal is injected into the grid voltage in the dq-domain. Both the grid control signal and the PRBS sequence have to be of the same length. This is due to generation and injection of the PRBS signal prior to starting of the measurement. The grid voltage reference has to start and end at the same voltage point which is in this experiment 0 V for phase a. This causes certain limitations to the generation frequency of the PRBS signal. The length of the PRBS sequence has to start when the phase a voltage is zero and end when the phase a voltage is zero. If this does not happen the grid voltage is not continuous.

The requirement that the PRBS signal and the grid voltage are synchronized limits the amount of different sampling frequencies which can be used in the experiment. The used sampling frequency can be calculated by using the grid frequency and the number of samples needed to perform the complete PRBS sequence. The sampling frequency f_{s} can be calculated with the following equation

$$f_{\text{s}} = [2 * (2^n - 1)] * \frac{f_{\text{g}}}{N_{\text{sin}}} \tag{3.10}$$

where $[2 * (2^n - 1)]$ presents the length of the PRBS sequence with each of bits given twice to prevent aliasing, f_{g} the grid frequency and N_{sin} number of grid voltage waveform sequences within one PRBS sequence. This is then multiplied with the frequency of the grid f_{g} and divided by the number grid waveform sine periods that the complete PRBS sequence takes to complete. Table 3.2 has some of the possible sampling frequencies.

Table 3.2 *Maximum sampling frequencies for different length PRBS signal when maximum sampling frequency is 250 kHz*

PRBS Bits	PRBS Length	Grid Frequency	Number of Grid Waveform Periods	Sampling Frequency
12	4095	50	2	204 750 Hz
12	4095	60	2	245 700 Hz
13	8191	50	4	204 775 Hz
13	8191	60	4	245 730 Hz
14	16383	50	7	234 050 Hz
14	16383	60	8	245 745 Hz
15	32767	50	14	234 050 Hz
15	32767	60	16	245 753 Hz
16	65535	50	27	242 722 Hz
16	65535	60	32	245 756 Hz

The values for the sampling frequency in Table 3.2 are calculated so that the sampling frequency is as close to 250 kHz as possible. 250 kHz is the maximum sampling frequency that the NI-DAQ Data Acquisition card can perform. Using large values for the number of bit when generating PRBS gives better resolution to the measurement but each bit doubles the length of the signal. This is a tradeoff between accuracy of the experiment and needed calculation power and time. The frequency values have also been rounded to the nearest integer value. The rounding causes a maximum of 0.001221 Hz error in the grid frequency with the values used.

3.6 Verification of the Measurement Setup

The system being built is measuring the output impedance of the inverter to higher frequency bandwidth than the system tied to the switching frequency of the inverter. The bandwidth of the measurement is significantly higher than the highest possible measurement bandwidth with the system tied to the inverter. A method to verify the measurement accuracy was created. This was done by measuring the frequency response of a simple RL- and RLC-circuits and checking if the form of the results matches with the theoretical model and how is the accuracy compared to a measurement made with the combination of dSPACE real-time simulation and Venable frequency response analyzer. Rough approximation of the amount of noise produced

by the grid emulator to the measurement can be made by comparing different averaging methods; mainly time averaging and Cross-spectrum method. Background noise caused by the experiment setup can be negated from either input or output signal by using Cross-Spectrum averaging the results. The use of these two methods can be seen from Fig. 3.5.
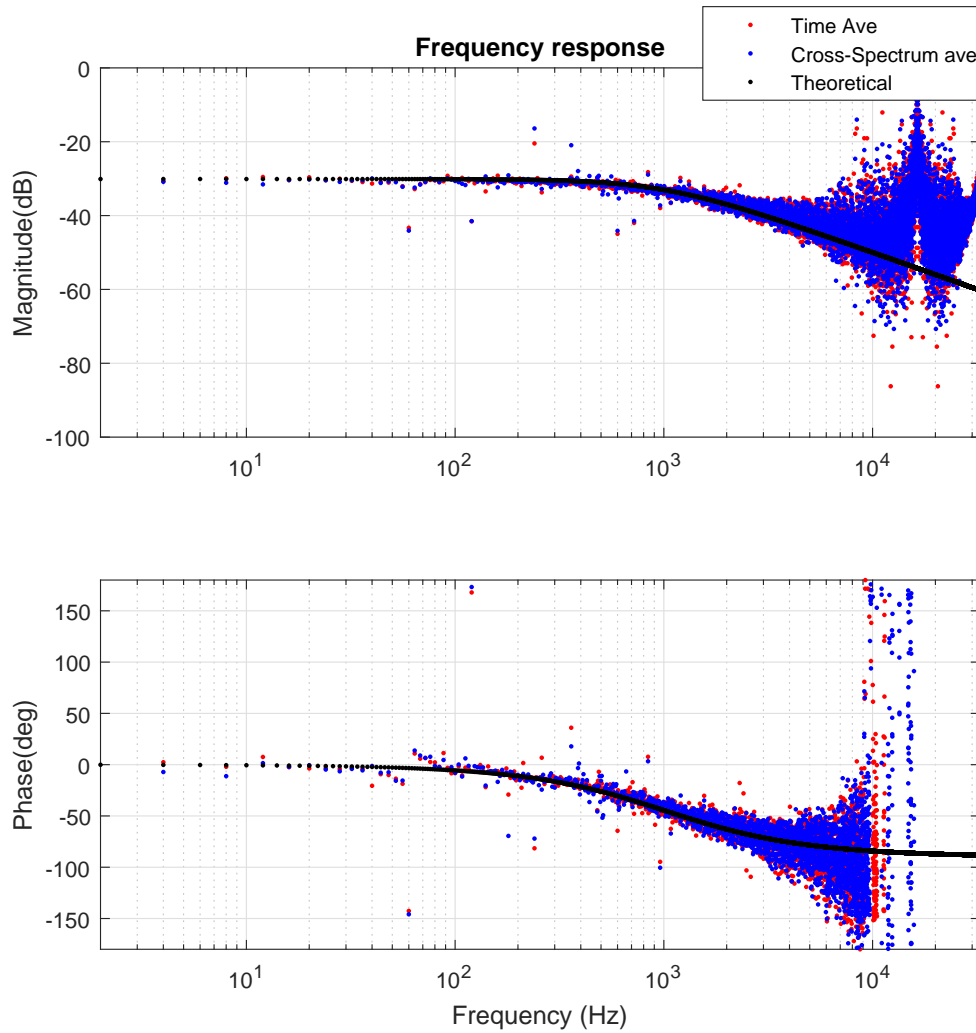

Figure 3.5 *32 kHz Frequency response test with an RL-circuit*

Fig. 3.5 shows the results of the PRBS frequency response test. This measurement was done by connecting each phase of the the grid-emulator to a 32,3 Ω resistance and 5 mH inductor and setting them into a star-connection. The used circuit is shown in Fig. 3.6.
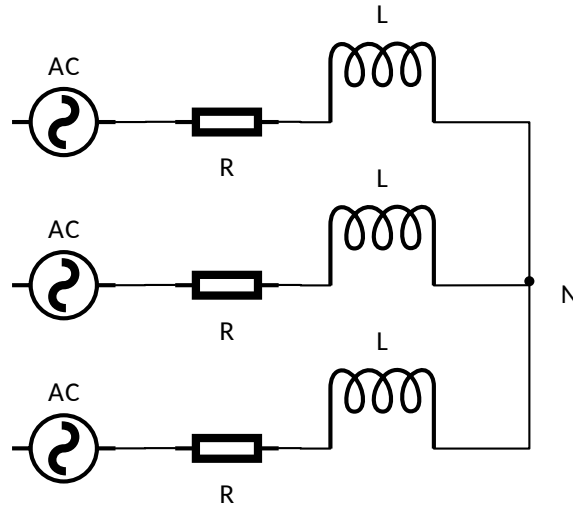
Figure 3.6 *RL-circuit used in the test*

As the tested circuit is a passive circuit with only two components the reference model is easy to produce. The reference value is calculated by the following equation in Laplace-plane

$$G = \frac{1}{R + L * s} \tag{3.11}$$

where R is the resistance and L is the inductance of connected components. Used sampling frequency in the test is 32 kHz and this limits the PRBS generation to Nyquist frequency which is 16 kHz. As stated in chapter 2 the PRBS is accurate up to around 1/2.5 or 1/3 of its generation frequency. In this case the upper limit of the accurate frequency range is between 5.3 and 6.4 kHz. Measured gain values begin to deviate from the theoretical value after 6 kHz point as expected. Same happens to the phase value. After 6 kHz the measured value for the phase starts to scatter far from the theoretical value. The difference between the two averaging methods is not large due to the fact that the cross-correlation method was set to remove noise from the output. The used circuit is a simple passive RL-circuit which does not produce great amounts of noise.

This test was repeated with different sampling frequencies for both a RL-circuit and RLC-circuit. The used RLC-circuit was made by adding a 25 μF capacitor into the RL-circuit. The following schematic in Fig. 3.7 shows the used test circuit.
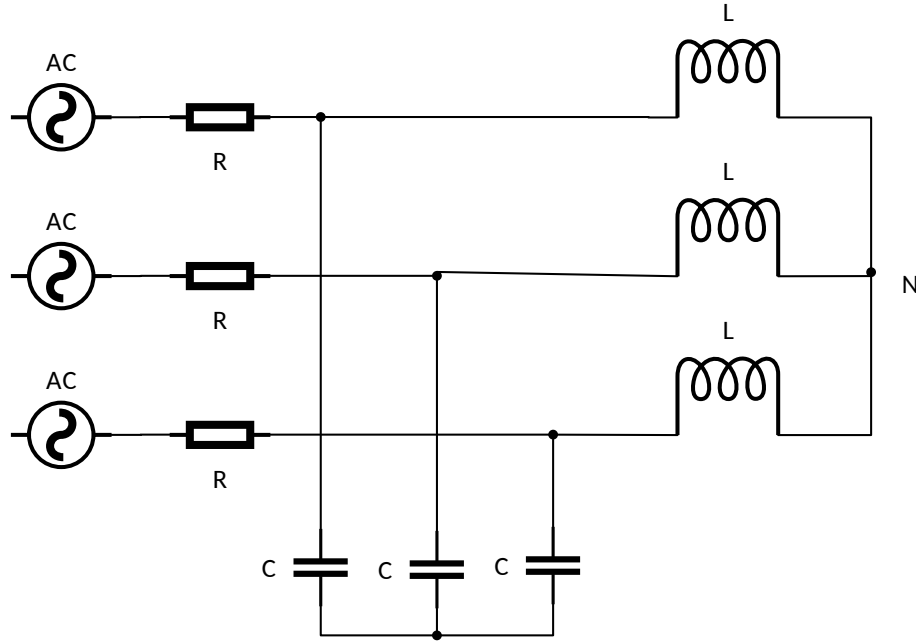
Figure 3.7 *RL-circuit used in the test*

The used RLC-circuit is a layout of a basic low-pass filter which filters out frequencies above its bandwidth. There is a peak in the gain waveform at the resonant frequency of the filter. Reference value is calculated by forming a transfer function $i_{\text{in}}/v_{\text{in}}$ for single phase equivalent circuit assuming symmetrical voltages and load. The reference points for the measurement are calculated by changing the component values in to Laplace-domain. Inductor becomes sL, the capacitor $1/sC$ and resistor is R. These values are then used to calculate the input admittance transfer function which is

$$Y_{\text{in}} = \frac{i_{\text{in}}}{u_{\text{in}}} = \frac{sRC + 1}{s^2 RLC + sL + R} \tag{3.12}$$

Figs. 3.8 and 3.9 shows the measured frequency response for the admittance measurement of the circuit. All of the measurements are made with 13-bit PRBS injected into grid voltage of 50 Volts and 50 Hz.
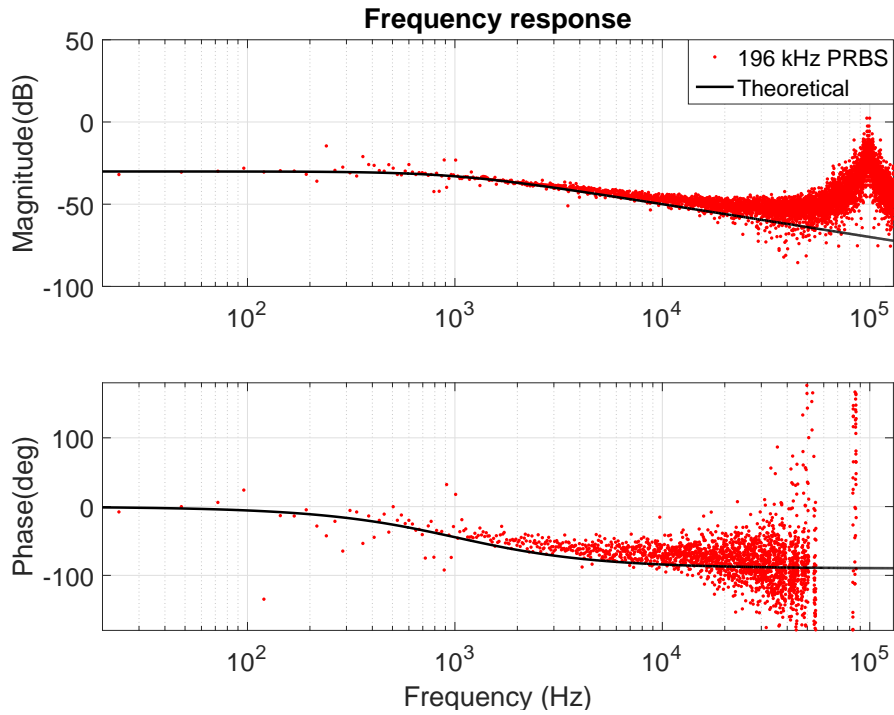
(a) 196584 Hz Sampling frequency RL-circuit.
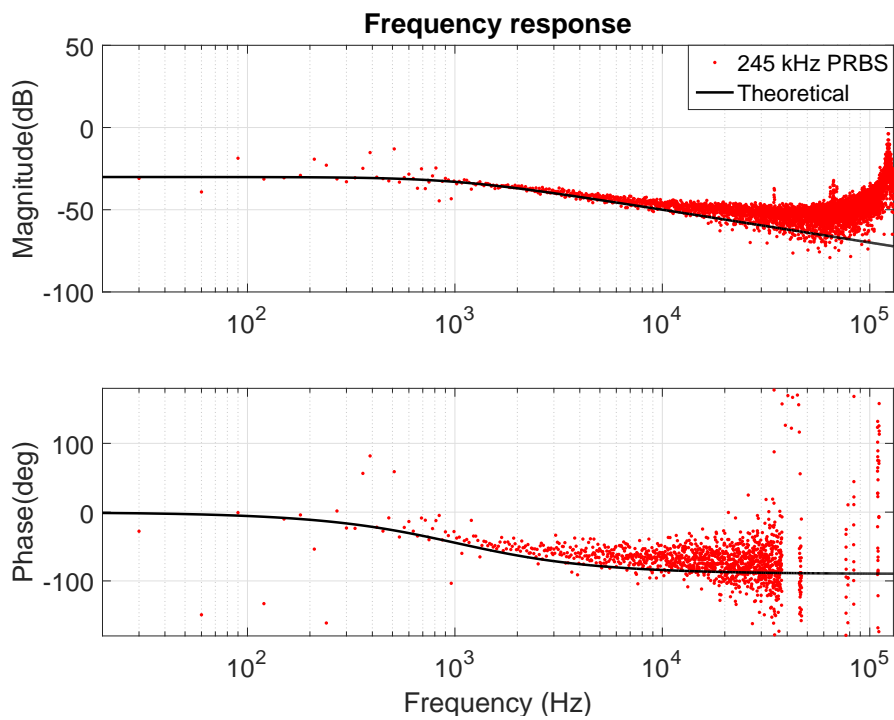
(b) 245730 Hz Sampling frequency RL-circuit.

Figure 3.8 *Reference tests made to determine the accuracy of the measurement with a RL-circuit*
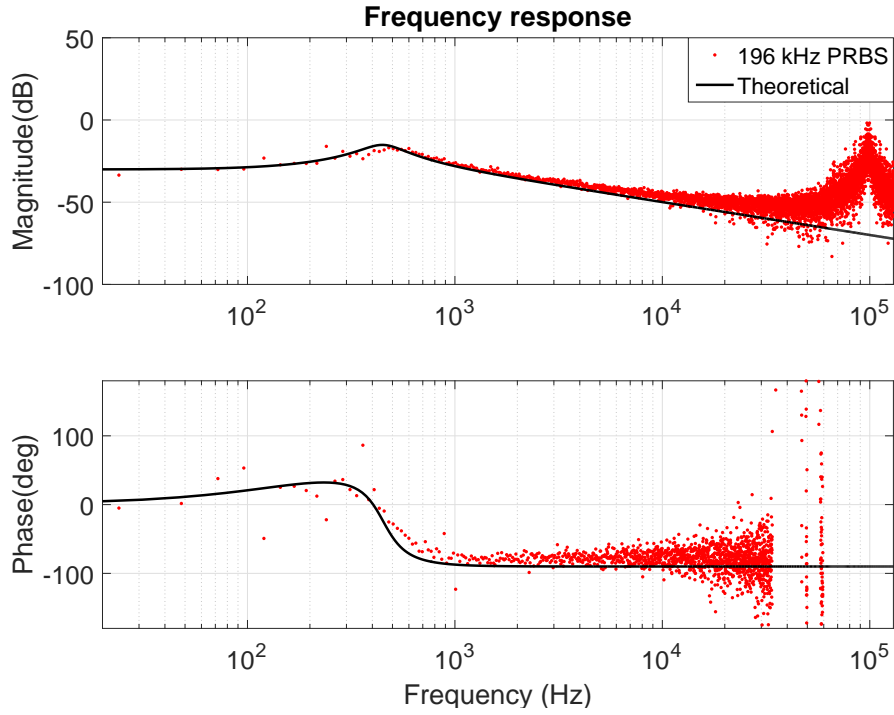
(a) 196584 Hz Sampling frequency RLC-circuit.
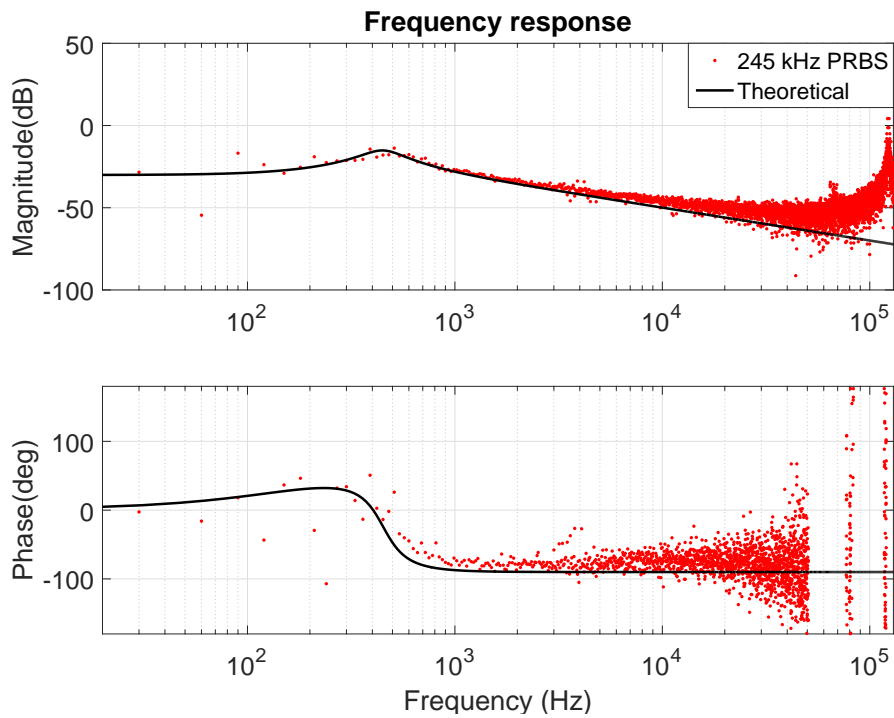
(b) 245730 Hz Sampling frequency RLC-circuit.

Figure 3.9 *Reference tests made to determine the accuracy of the measurement with a RLC-circuit*

From Figs. 3.8 and 3.9 we can see that the impedance measurement stays reasonably close to the reference line with RL- and RLC-circuit up to 1/3 of the generation frequency of the PRBS. However when measuring with higher frequency PRBS the measurements at low frequencies start to scatter and become unreliable. This could be caused by the internal functioning of the measurement card or the grid emulator as both of the devices are operated near their maximum capability.

Overall the measurements made for a passive circuit can be considered accurate enough for making the impedance measurement with PRBS and all of the equipment used is still capable of operating at these levels of sampling frequency. The reference values used can be considered accurate as the tested circuit is passive and its design is simple. The passive components were not measured for their real values but manufacturers have stated all of the components to be within 5% of the given value.

3.7   Error Caused by the Measurement Card

There are errors in the measurements done in test which cannot be accounted for prior to knowing the equipment in use. There are delays in the measurement and the fact that the experiment done requires 3 outputs and 4 input which are preferably done simultaneously while using high frequencies for the sample rate causes errors from the internal operation of the measurement card. The measurement card used in this thesis is NI-DAQ USB-6363 which does not support simultaneous data acquisition from its input channels. The NIDAQ-6363 works by acquiring a value from one input at a time and when the sampling period is over the process is repeated. The way this works in our measurement is demonstrated in the following figure.
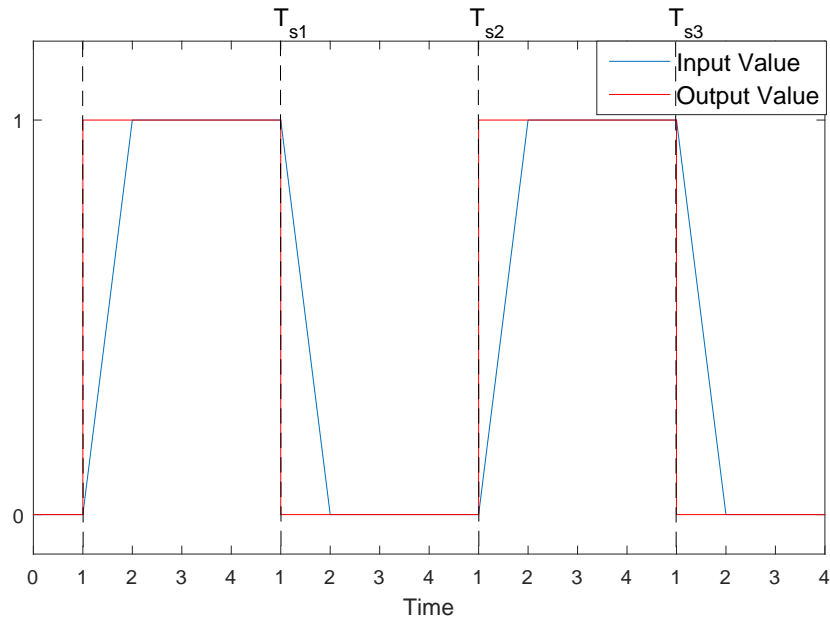
Figure 3.10 *Data acquisition error*

The way the data is gathered is presented in Fig. 3.10. There is delay in the system which means that the measured values in input channel 1 haven't had enough time to be updated to the new control point before the new values is taken. This causes that the channel 1 value always lags one period behind other measurements. This has severe effects on the results of the frequency response analysis. The phase shift of the signal doesn't represent the real value as can be seen from the Fig. 3.11.
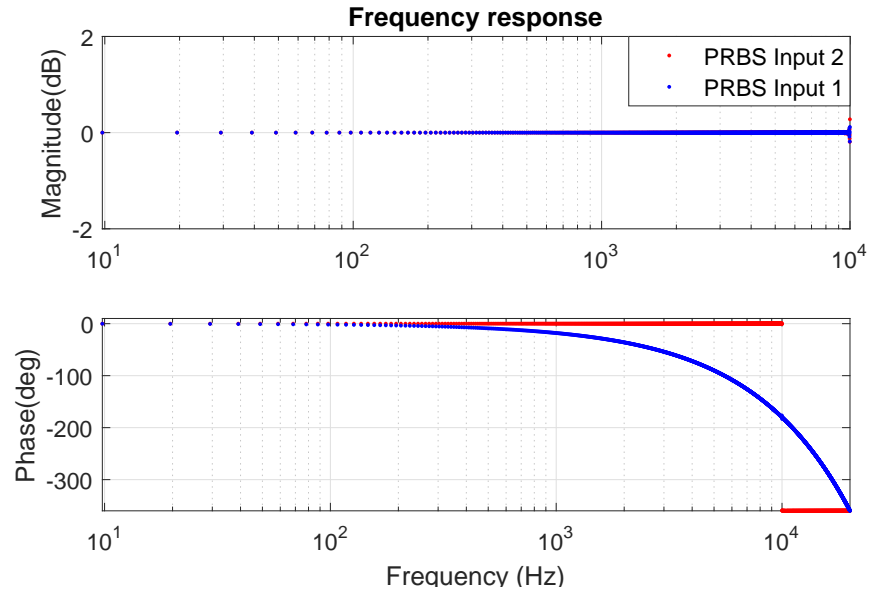
***Figure 3.11** Phase shift error in the frequency response*

In Fig. 3.11 a PRBS signal voltage is measured over a resistance and compared to the reference value. As the values of the first channel are a complete period behind the other channels used there is a 360 degrees phase shift from 0 Hz to the sampling frequency of the device. This additional phase shift increases linearly and is positive or negative depending on how the measurement probes are connected to the measurement card. This has to be taken into account when making the measurements needed for the experiment. There is also some phase shift caused by the fact that the measurements are not simultaneous. The non-simultaneous measurements can be negated by taking all of the measurements close to the start of the sampling period. This works when the needed sampling frequency is much lower than the limits of the equipment. However for this thesis the measurement card is operating at its limits and this can cause some distortion to the phase shift.

In this thesis the error caused by the internal functioning of the DAQ-device is negated by removing the false data from the data set. The length of the complete measurement is increased by 1 bit to allow the use of complete PRBS sequence for the averaging. From the first channel the first data point is removed and from the other channels the last point is removed. This makes the measured data synchronized due to the fact that output values are discrete and remain the same until the next sampling sequence.

3.7.1   Quantization error

The resolution of the measurements have finite accuracy and this causes error to the gain of the frequency response analysis when the measured changes in the voltages and currents are very small. Table 3.1 states that the resolution of the USB-6363 DAQ measurement card is 16 bits. This means 65536 different possible states between the minimum and maximum values of the measurement range. Resolution of the measurement can be defined by

$$V_{\text{res}} = \frac{V_{\text{range}}}{2^n} \tag{3.13}$$

Where V_{res} is the resolution of the measured voltage, V_{range} is the difference between maximum and minimum values possible to measure and n is the number of bits in the PRBS. The measured voltage ranges between -325 V and 325 V for 230 V grid and the current is at maximum for 10 kVA system around 20 A. Voltage probes have a gain of $1/100$ and current probes have a gain of $1/10$. The measured values sent to the measurement card are between -3.25 and 3.25 for voltage and -2 and 2 for current. The used range with the data acquisition card is -5 V to 5 V. With this range the resolution V_{res} is $1.5259 * 10^{-4}$ V. The impedances calculated for the inverter at high frequencies can have high values which means that the measured change in current can be very small and the impedance value calculated could be distorted by the error in measurement. In Figs. 3.12 - 3.14 different amplitude PRBS-signals with cross-spectrum averaging are tested over an RL-circuit to gain the admittance value of the test circuit. The measurements are done by averaging 50 sequences of the PRBS signal.
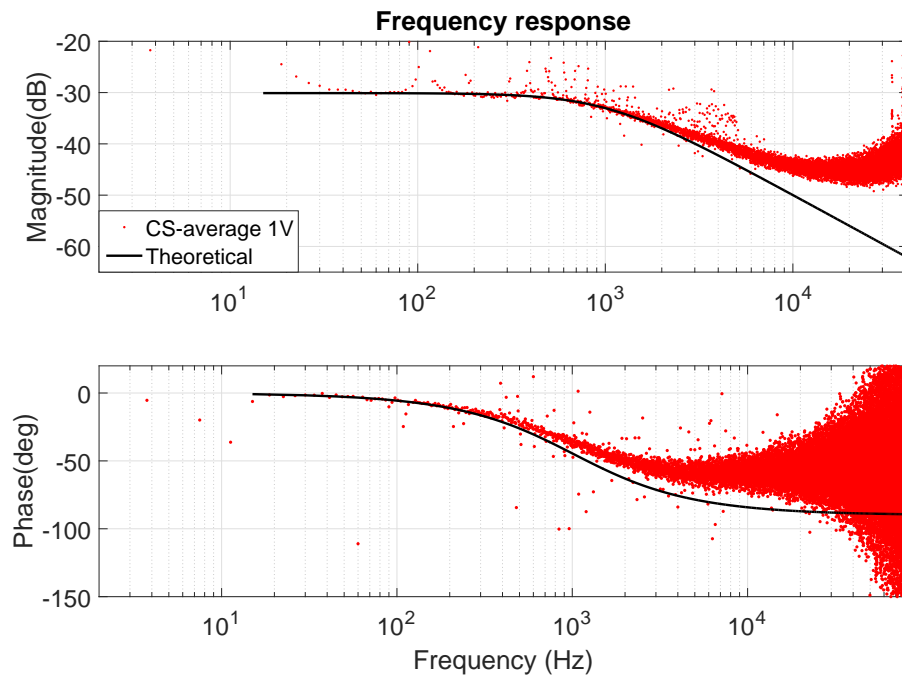
Figure 3.12 *Frequency response analysis with cross-spectrum averaging with 1 V PRBS amplitude*
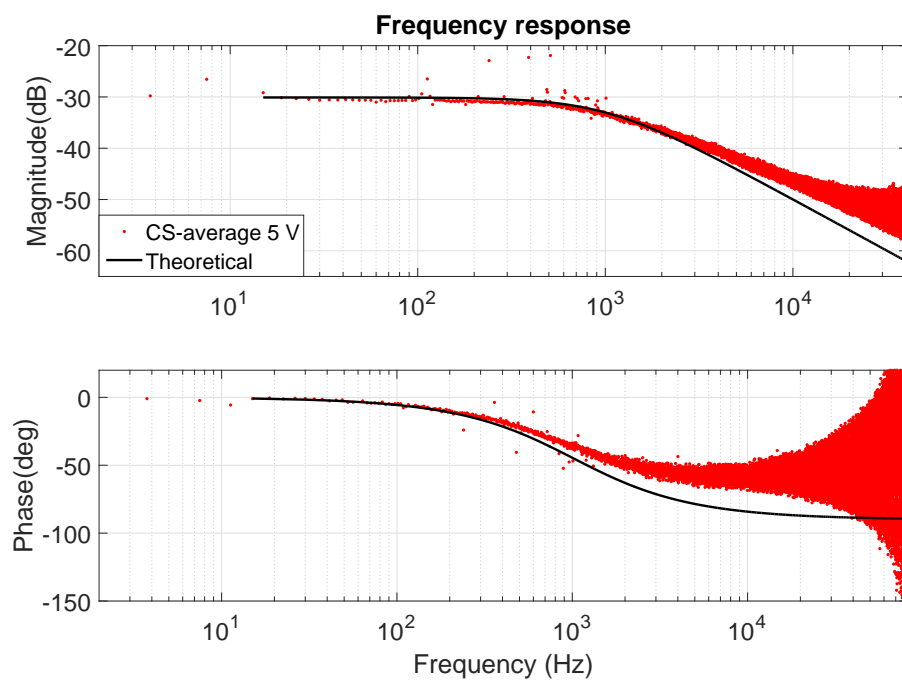

Figure 3.13 *Frequency response analysis with cross-spectrum averaging with 5 V PRBS amplitude*
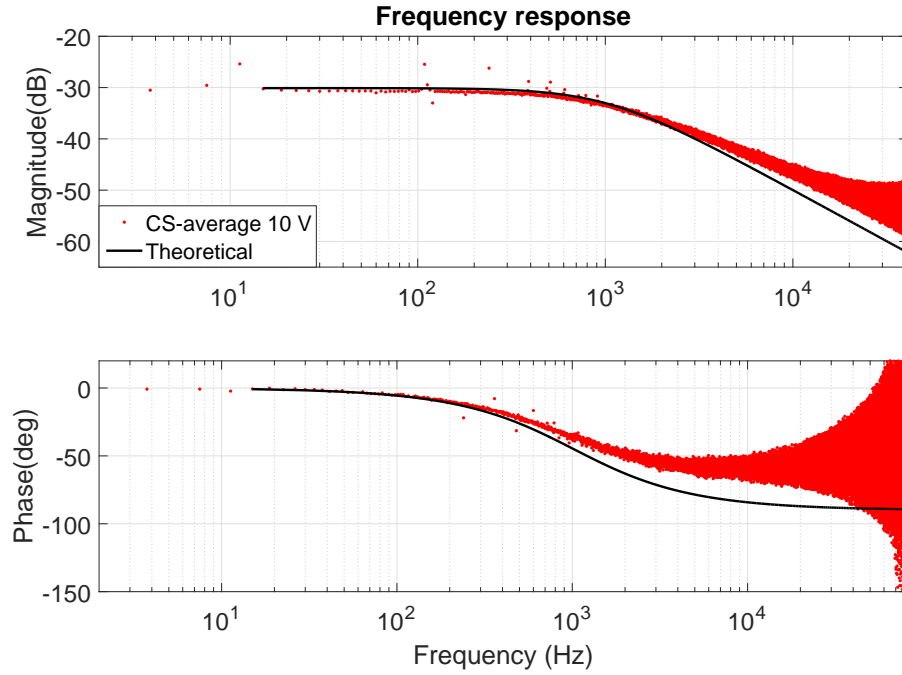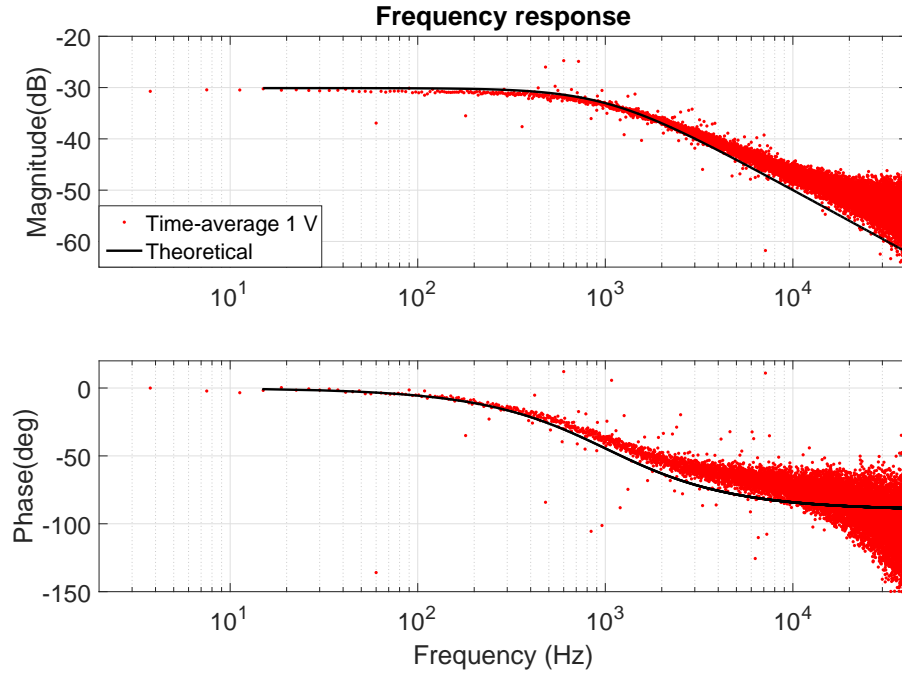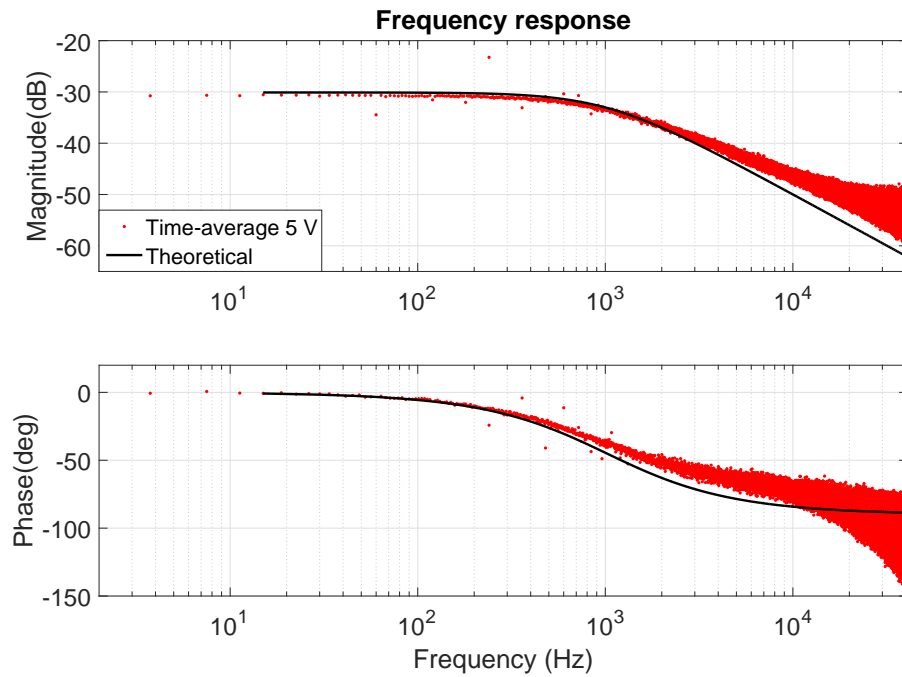
Figure 3.14 *Frequency response analysis with cross-spectrum averaging with 10 V PRBS amplitude*

The effect of the limited accuracy in the measurements is seen from the deviation of the calculated value from the theoretical value at lower frequency than it should. -40 dB values is the limit for the 1 V PRBS signal and for the 5 V and the 10 V signals the limit is much lower. The energy of the PRBS signal has to be considered when making the measurements as the measurements have finite accuracy. The same test was done with time averaging shown in Figs. (3.15-3.17).

Figure 3.15 *Frequency response analysis with cross-spectrum averaging with 1 V PRBS amplitude*

Figure 3.16 *Frequency response analysis with cross-spectrum averaging with 5 V PRBS amplitude*

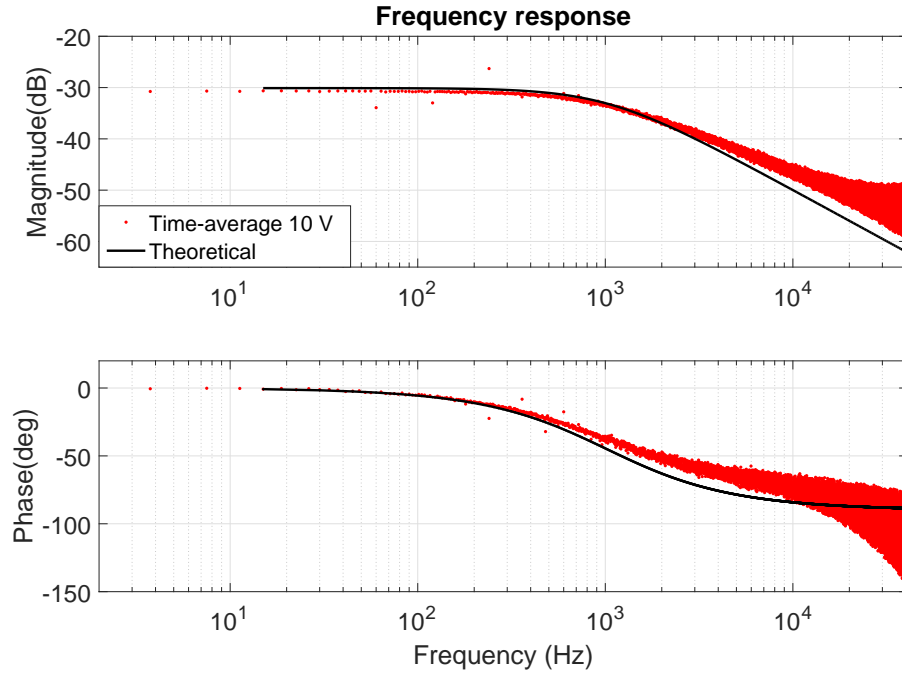***Figure*** ***3.17*** *Frequency response analysis with cross-spectrum averaging with 10 V PRBS amplitude*

The time averaging is much less susceptible to the inaccuracy of the measurements and the increase of the PRBS signal amplitude only improves the measurement by reducing the scattering of the points. This means that the time-averaging is better when the measured changes are very small compared to the range of the measurement. This could be due to time averaging removing some of the quantization effect.

4.   INVERTER IMPEDANCE MEASUREMENTS

Frequency response analysis gives detailed information about the system being tested. For this experiment the control of the grid-side of the setup is separated from the inverter control which allows the use of higher frequencies than the switching frequency of the inverter. Goal of this experiment is to measure the impedance at frequencies over the inverter switching frequency.

4.1   Grid and PV parameters

The tests are made with a certain set of system parameters such as input current and voltage because changing these parameters results in a different inverter impedance. The impedance has to remain unchanged so that the results are comparable. Electrical parameters used in the system are presented in Table 4.1 and the control parameters of the inverter are presented in Table 4.2. These parameters are used in both the measurements made with the PRBS signal and the measurements made with a network analyzer (Venable) based on sine-sweep method.

Table 4.1 Electrical parameters

Electrical Parameters	Values
L Filter	2,5 mH
DC-capacitor	1,5 mF
DC-link Voltage	420 V
AC Voltage	120 V_{rms}
Grid Frequency	60 Hz

Table *4.2 Control Parameters of the inverter*

Control Parameters	Values
Switching frequency f_s	12 kHz
Current controller K_p	0.0273
Current controller K_i	34.2768
PLL K_i	38.0189
PLL K_p	0.6723
PLL crossover frequency	20 Hz

The photovoltaic emulator is set to a certain power curve with maximum power point at 420 V. The with PLL bandwidth set to 20 Hz. There's is no voltage feedforward activated on the control system although it is possible to do so.

4.2 Frequency Response

The output current and voltage of the inverter were measured. Output impedance of the inverter is calculated by comparing these values and applying frequency response analysis. Figs. 4.1 - 4.4 present the measured impedance values for d and q components of the voltages and currents of the system. The calculations are made with both time averaging and cross-spectrum averaging. The impedance waveform is compared to measurements done with sinewave perturbation signal. The voltage and current d or q component depending on the measurement is removed from the results and this is sent through a DAC back to Venable for frequency response analysis. The reference measurement made by sinewave perturbation is made only up to 6 kHz. The sampling frequency of the dSPACE restricts the maximum frequency possible to be used for the frequency response analysis. The dSPACE uses a certain inverter switching frequency as its sampling frequency. For this experiment the switching frequency is 12 kHz as shown in Table 4.2. The maximum measurable frequency is stated to be Nyquist frequency which is half of the sampling frequency. The reference is accurate only to 6 kHz.
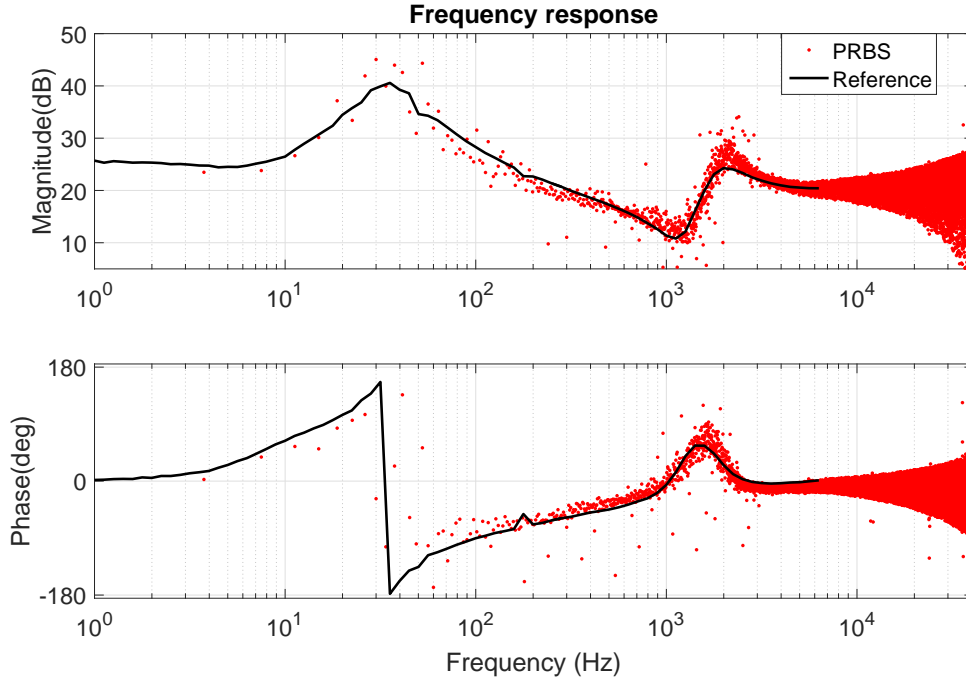
Figure 4.1 *Inverter output impedance d-component with time averaging*

The transfer function between output current d component and output voltage d component is shown in Fig. 4.1. The measurement is done with 245730 Hz sampling frequency which means 122715 Hz generation frequency for the PRBS signal. This gives theoretically accurate measurement bandwidth of about 40670 Hz. The resolution of the measurement is 4 Hz as the PRBS signal is divided over 16 periods of the grid frequency. The measurements are following accurately following the references. After 6 kHz the reference measurement is no long accurate due to the limitations in the measurement setup. There are some distortion at the grid frequency and multiples of it but that is expected as the measured signals are composed mostly of these components. The measurements and calculated impedance points begin to spread after 10 kHz and by the theoretical limit of 40 kHz the impedance gain value has points that differ 20 dB of each other and phase points which differ 100 degrees. The measurements are not accurate when the measured frequency is close to the theoretical limit but the values are still following right path. In Fig. 4.2 the same measurements are made for the inverter output impedance q-component.
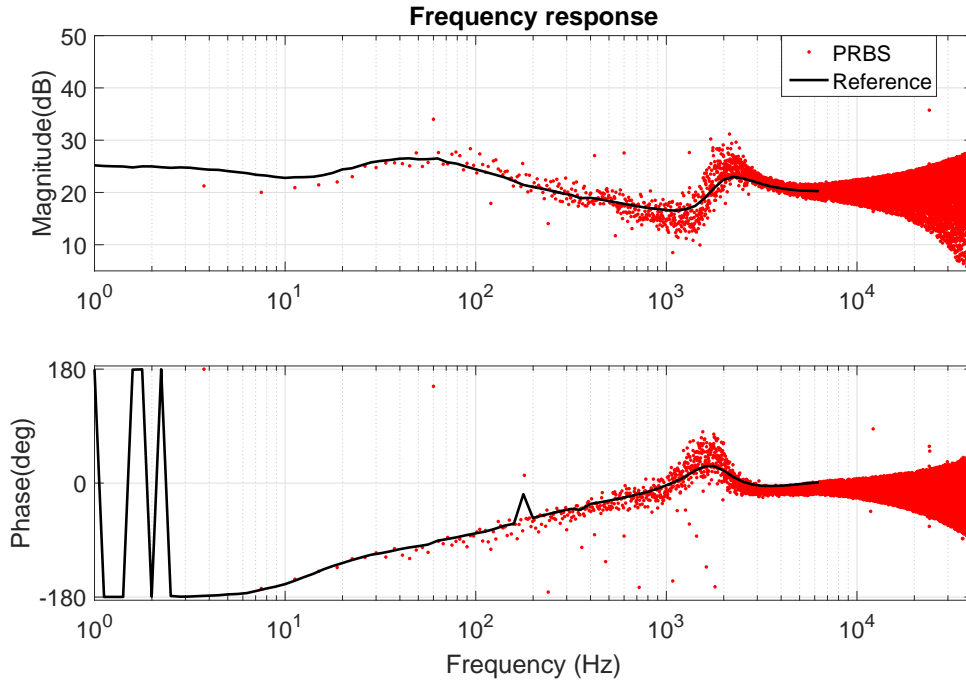
Figure 4.2 *Inverter output impedance q-component with time averaging*

The impedance for the q-component is following the reference value accurately. Same as with the d-component the measurements begin to spread after 10 kHz. The measurements are following the reference at both low and high frequencies and can give approximate values from the whole spectrum on one measurement set. As stated in [21] cross-spectrum averaging is expected to be more accurate than time averaging. This can be seen in Figs. 4.3 and 4.4
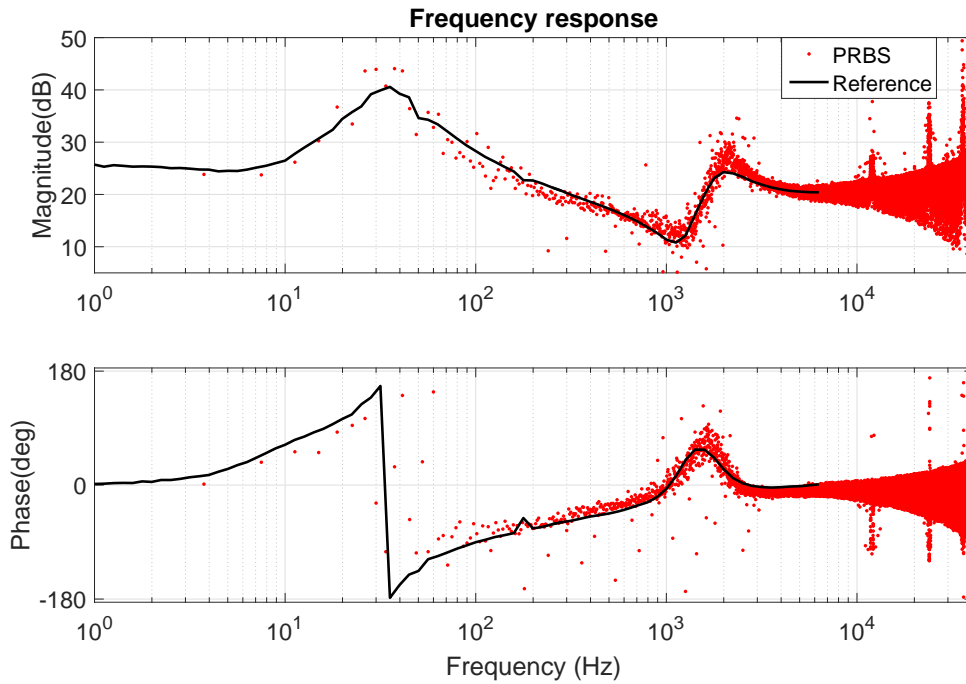
Figure *4.3 Inverter output impedance d-component with cross-spectrum averaging*

The measurements follow the reference value and have slightly smaller spread than the time averaging method. The phase value measurements are tighter than its counterpart on the time averaged measurements. The disturbance at the grid frequencies are stronger than with the time averaging which can be seen as the large spikes at 60 Hz and its multiples. The measurements are averaged 50 times which might be the cause of no visible difference between the averaging methods.
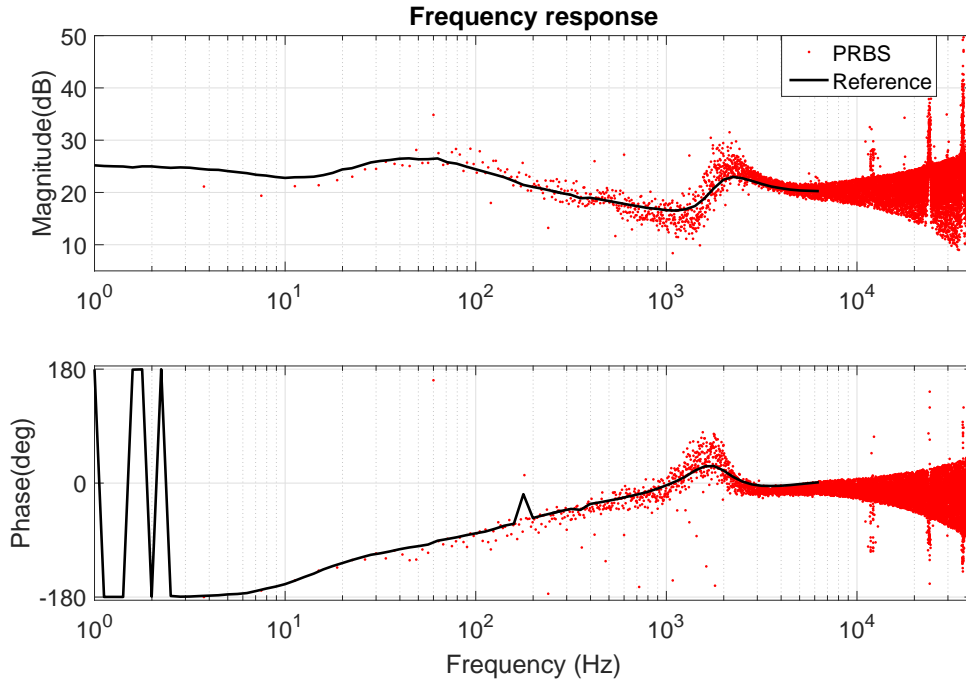
Figure *4.4 Inverter output impedance q-component with cross-spectrum averaging*

The inverter output impedance q-component measurements with cross-spectrum averaging have similar differences to the time averaged version as the d-component measurements. The measured impedance curve is almost the as the time averaged version and disturbances at the grid frequency and its multiples are stronger.

The PRBS used to do the measurements is injected on top of the d- or q-component of the grid voltage. The effect of a PRBS signal to the voltage and current with amplitude of 15 V is seen in Figs. 4.5 and 4.6. The voltage and current waveforms without the perturbation signal is shown for comparison.
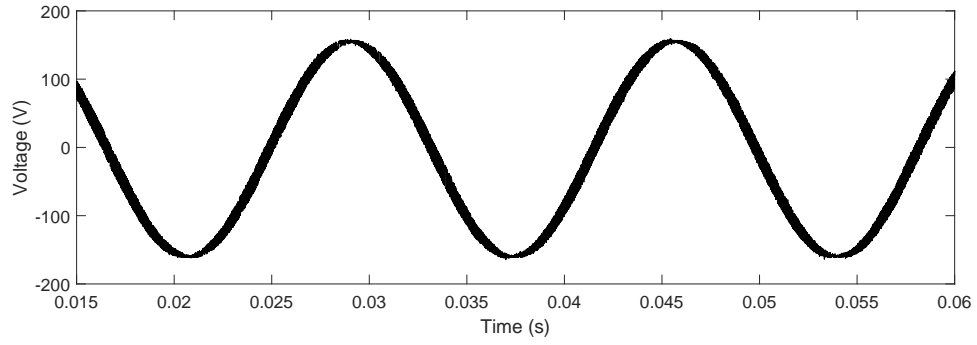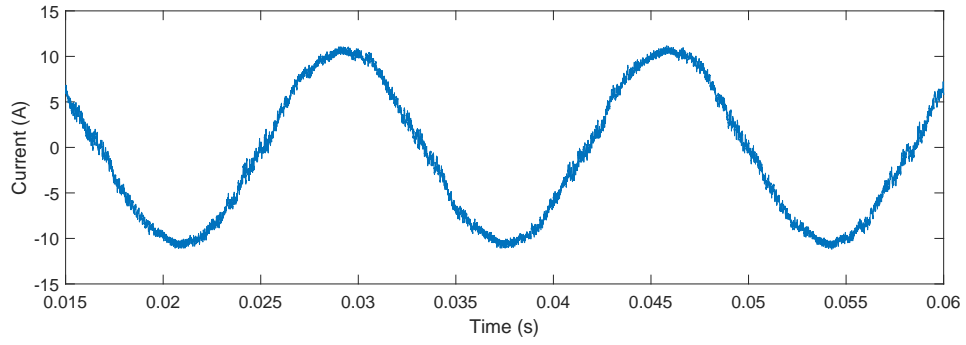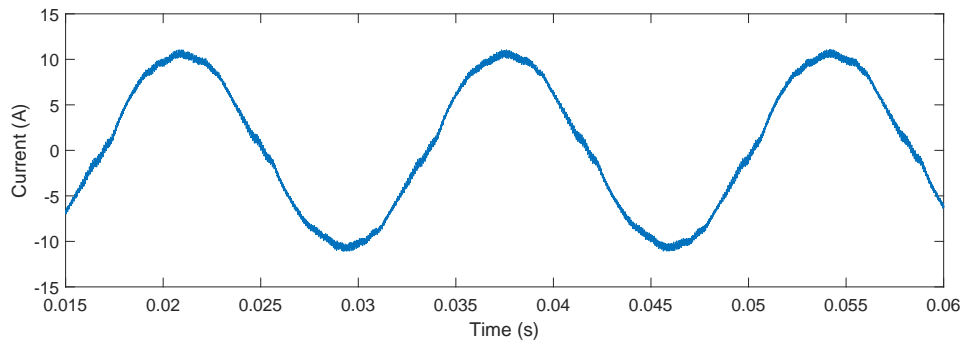
(a) Phase A voltage with PRBS injection.
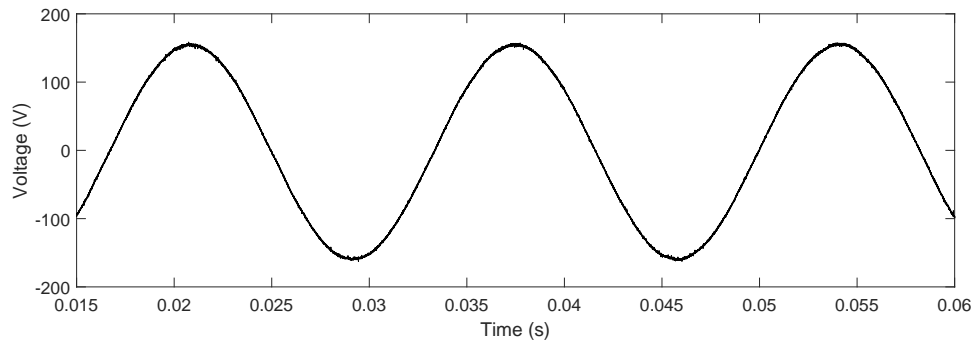
(b) Phase A voltage without PRBS injection.

Figure *4.5 Grid voltage waveforms with and without PRBS injection*

The voltage figure for phase a in Fig 4.5 is still close to the basic grid frequency voltage even when there is a PRBS signal with generation frequency of 122865 Hz and amplitude of 15 V.

(a) Phase A current with PRBS injection.

(b) Phase A current without PRBS injection.

Figure 4.6 *Grid voltage waveforms with and without PRBS injection*

The currents are shown in Fig. 4.6 with and without the PRBS injection. The one with PRBS has only slightly more distortion than the one without the PRBS. Most of the distortion of the wave form is caused by the inverter operation not the injection of the PRBS signal.

5. CONCLUSIONS

The implementation of the impedance measurement setup using PRBS signal as the perturbation signal was successful. The measurements follow the theoretical value quite well and there is only slight deviation from the reference value. The limitations on the test setup causes the maximum bandwidth of the reference measurement to be 6 kHz while the system being tested in this thesis is theoretically accurate up to around 40 kHz. The limitation in the previous setup leaves leaves the large part of the measurements made on the inverter unverified. However the measured curve for both the d-component and q-component of the inverter output impedance are following a curve at higher frequencies than 6 kHz and the test measurements made on passive circuit were accurate to higher frequencies.

Passive circuit and a theoretical values for the impedance values can be used as a reference for the new test setup. The measurements made with PRBS followed the theoretical value of the circuit quite well but the measurements aren't accurate as far as the theory states. There are multiple reasons why the measurements are not accurate to the point which they should be. There are a lot of noise taken into the measurements when using real components and not only simulations. The measured impedance is taken over a large area of frequencies and the measured signal variation at the certain frequency can be minimal as the energy of the PRBS signal is spread over the whole bandwidth.

Overall the measurement setup works as intended and gives results that are accurate enough and can easily be scaled to the required bandwidth, resolution and accuracy. Increasing signal strength and the number of averaged sequences gives the measurements more accuracy while the signal length and frequency the resolution and bandwidth. The measurements can be integrated to a separate DSP board to allow online control of the signals and are not limited to certain equipment. Same principle of PRBS and impedance calculations work regardless of the equipment used. The equipment only gives the limitations of the measurement.

BIBLIOGRAPHY

[1] M. Youhannaei, H. Mokhtari, and A. Sharifi, The effects of widespread use of power-electronic based dg on grid power quality, 23rd International Conference on Electricity Distribution, (Paper 0377), June 2015.

[2] J. H. R. Enslin and P. J. M. Heskes, Harmonic interaction between a large number of distributed power inverters and the distribution network, IEEE Transactions on Power Electronics, vol. 19, no. 6, pp. 1586-1593, 2004.

[3] M. Liserre, R. Teodorescu, and F. Blaabjerg, Stability of photovoltaic and wind turbine grid-connected inverters for a large set of grid impedance values, IEEE Transactions on Power Electronics, vol. 21, no. 1, pp. 263-272, 2006.

[4] T. Basso and F. Goodman and J. Koepfinger and C. Vartanian and M Kipness, IEEE 1547 Standard for Interconnecting Distributed Resources with Electric Power Systems, IEEE, 2013.

[5] Robin Grab, Soenke Rogalla, Roland Singer, and Gregor Doetter, Testing pv central inverter's compliance with international grid codes, Journal of Energy and Power Engineering, pp. 1552-1558, 2014.

[6] J. Sun, Impedance-based stability criterion for grid-connected inverters, IEEE Transactions on Power Electronics, vol 26, no. 11, pp. 3075-3078, Nov 2011.

[7] M. Cespedes and J. Sun. Three-phase impedance measurement for system stability analysis. In Control and Modeling for Power Electronics (COMPEL), 2013 IEEE 14th Workshop on, pp. 1-6, June 2013.

[8] T. Roinila, M. Vilkko, and J. Sun, Broadband methods for online grid impedance measurement, In 2013 IEEE Energy Conversion Congress and Exposition, pp. 3003-3010, Sept 2013.

[9] D. Martin, I. Nam, J. Siegers, and E. Santi, Wide bandwidth three-phase impedance identification using existing power electronics inverter. In Applied Power Electronics Conference and Exposition (APEC), 2013 Twenty-Eighth Annual IEEE, pp. 334-341, March 2013.

[10] T. Roinila, M. Vilkko, and J. Sun, Online grid impedance measurement using discrete-interval binary sequence injection, In Control and Modeling for Power Electronics (COMPEL), 2013 IEEE 14th Workshop on, pp. 1-8, June 2013.

[11] T. Roinila, T. Messo, R. Luhtala, T. Reinikka, A. Aapro, and J. Sihvo, dSPACE implementation for real-time stability analysis of three-phase grid-connected systems applying MLBS injection, In Eurosim 2016, pp. 1-5, 2016.

[12] S. Milinkovic, Some applications of p-prbs signals in frequency domain measurements, In 2013 2nd Mediterranean Conference on Embedded Computing (MECO), pp. 204-207, 2013.

[13] M. Céspedes and J. Sun, Online grid impedance identification for adaptive control of grid-connected inverters, In 2012 IEEE Energy Conversion Congress and Exposition (ECCE), pp. 914-921, 2012.

[14] Z. Shen, M. Jaksic, P. Mattavelli, D. Boroyevich, J. Verhulst, and M. Belkhayat, Three-phase ac system impedance measurement unit (imu) using chirp signal injection, In Applied Power Electronics Conference and Exposition (APEC), 2013 Twenty-Eighth Annual IEEE, pp. 2666-2673, 2013.

[15] K. Godfrey, Perturbation Signals for System Identification, Prentice Hall International, 1993.

[16] A. Aapro, Modeling dynamics of photovoltaic inverter with lcl-type grid filter, Master's thesis, Tampere University of Technology, 2014.

[17] T. Messo, Factors Affecting Stable Operation of Grid-Connected Three-Phase Photovoltaic Inverters, PhD thesis, Tampere University of Technology, 2014.

[18] R. Dorf and R. Bishop, Modern Control Systems, Prentice Hall Inc, 9th edition, 2001.

[19] S. Vesti, T. Suntio, J. A. Oliver, R. Prieto, and J. A. Cobos, Impedance-based stability and transient-performance assessment applying maximum peak criteria, IEEE Transactions on Power Electronics, vol. 28, no. 5, pp. 2099-2104, 2013.

[20] B. Miao, R. Zane, and D. Maksimovic, System identification of power converters with digital control through cross-correlation methods, IEEE Transactions on Power Electronics, vol. 20, no. 5, pp. 1093-1099, 2005.

[21] T. Roinila, Fast Frequency Response Measurement Techniques in Analyzing the Dynamics of Switched-Mode Power Supplies. PhD thesis, Tampere University of Technology, 2010.

[22] A. Soni, Control-Relevant System Identification Using Nonlinear Volterra and Volterra-Laguerre Models, PhD thesis, University of Pittsburgh, 2006.

[23] G. Francis, R. Burgos, D. Boroyevich, F. Wang, and K. Karimi, An algorithm and implementation system for measuring impedance in the d-q domain, In 2011 IEEE Energy Conversion Congress and Exposition, pp. 3221-3228, Sept 2011.

[24] J. Jokipii, T. Messo, and T. Suntio, Simple method for measuring output impedance of a three-phase inverter in dq-domain, In 2014 International Power Electronics Conference (IPEC-Hiroshima 2014 - ECCE ASIA), pp. 1466-1470, May 2014.

[25] A. Aapro, T. Messo, and T. Suntio, An accurate small-signal model of a three-phase vsi-based photovoltaic inverter with lcl-filter, In 2015 9th International Conference on Power Electronics and ECCE Asia (ICPE-ECCE Asia), pp. 2267-2274, June 2015.